Statistical simulation of reentry capsule aerodynamics in hypersonic near-continuum flows

Mikhail S. Ivanov
Computational Aerodynamics Laboratory,
Khristianovich Institute of Theoretical and Applied Mechanics (ITAM),
Siberian Branch of the Russian Academy of Sciences,
Institutskaya 4/1, Novosibirsk 630090, Russia

24-28 January 2011

Summary

Current challenges and problems pertaining to the development and application of the DSMC method for high-altitude aerodynamics are discussed. Attention is paid to issues related to the efficiency and accuracy of the method in the near-continuum regime, as well as its use for modeling of rarefied flows with real gas effects. Accurate prediction of force and heat aerodynamic characteristics of reentry vehicles and spacecraft requires comprehensive investigation of hypersonic flows in the near-continuum regime. A powerful software system SMILE, which uses the direct simulation Monte Carlo method as a numerical approach and is built basing on the contemporary knowledge in this field, is developed to solve advanced problems of high-altitude aerothermodynamics. Effective numerical algorithms and physically grounded models of real gas effects are implemented in SMILE. Aerodynamics of promising reentry capsule in the near-continuum regime is considered as an example.

Contents

1 Introduction

The study of physical phenomena in rarefied nonequilibrium flows is a challenging problem directly related to the development of new aerospace technologies. Rarefied gas dynamics, that deals with these phenomena, is the synthesis of a great number of fundamental problems such as molecular collision dynamics and energy transfer phenomena in collisions, gas-surface interactions, condensation and evaporation, plume and expansion flows, and many others. All these problems are in close connection with applied, practical issues that can be conventionally divided into two groups. The first group covers the questions related to aerodynamic calculations of hypersonic flight of vehicles at high altitudes, the second group being mainly represented by the problems that involve the calculation of nozzle flows in thrusters and jets exhausting into vacuum and interacting with the surface of space objects.

Substantial difficulties arising in the study of such flows are caused by both the problems related to rarefaction and physico-chemical effects. It is commonly known that experimental simulation of nonequilibrium low-density flows is rather problematic and expensive. The difficulties of experimental modeling have stimulated an intense development of various approaches for numerical simulation of these flows. Presently there are numerous numerical approaches for solving the problems of rarefied gas dynamics, and the choice of this or that approach depends usually on the flow rarefaction, the problem dimension and the presence of real gas effects.

The choice of the numerical approach to be used to model rarefied nonequilibrium flows greatly depends on the extent of flow rarefaction. For near-continuum flows, it is usually sufficient to take into account the initial effects of rarefaction through the boundary conditions of slip velocity and temperature jump on the surface. The Navier-Stokes or viscous shock layer equations are commonly used with these boundary conditions. The Navier-Stokes equations can be derived from the Boltzmann equation under the assumption of small deviation of the distribution function from equilibrium. Therefore, they become unsuitable for studying rarefied flows where the distribution function becomes considerably nonequilibrium.

To study rarefied flows with a significant degree of nonequilibrium, the Direct Simulation Monte Carlo (DSMC) method is usually employed. This method has become the main technique for studying complex multidimensional rarefied flows. It has been successfully applied over the last four decades to model various flow phenomena and gas dynamic problems. The method has gradually evolved to the stage where its application to calculate complex three- dimensional flows is almost straightforward. The extended area of applicability of the DSMC method is from the near-continuum regime where it overlaps with that of the continuum approaches, to the free-molecular regime. In practice, the DSMC method is computationally intensive compared with its continuum counterparts. However, with increasing capabilities of modern parallel computers this method acquires new areas of application, such as modeling of internal and external near-continuum flows, detailed study of different three-dimensional problems with real gas effects, and others.

The Laboratory of Computational Aerodynamics from the Khristianovich Institute of Theoretical and Applied Mechanics of the Siberian Branch of the Russian Academy of Sciences has more than decade-long experience in the development of the DSMC method.

The result of these efforts is a computational system called SMILE (Statistical Modeling In Low-Density Environment) capable of solving a very wide range of basic and applied problems. The SMILE system provides a complete lifecycle of computations starting from a geometry model, pre-processing, going through the computation proper, and finishing with post-processing and presentation of results. All SMILE subsystems have a Graphic User Interface (GUI), which makes them user-friendly and easy to use. The SMILE core code is written in FORTRAN90 and has no memory limitations specific to static FORTRAN programs. The user interface of the system is written in C++ and uses a free cross-platform wxWidgets GUI library. The same theoretical basis (majorant collision frequency schemes) is used to develop more advanced software systems RGDAS and SMILE++.

The principal objectives of the paper are to analyze the modern status of the DSMC method, outline promising directions of method development, discuss problems that may be encountered, and give possible ways to overcome these problems. The paper discusses modeling of real gas effects, the numerical accuracy issues for the DSMC method, and application of the SMILE software system for studying promising capsule aerodynamics.

2 Conceptual issues of the DSMC method

The DSMC method is traditionally considered as a method of statistical simulation of the behavior of a great number of simulated gas molecules. Usually the number of simulated particles is large enough ($\sim 10^5 - 10^8$), but this is extremely small in comparison with the number of real molecules. Each simulated particle is then regarded as representing an appropriate number of actual molecules, F_{num}.

The main principle of DSMC is the splitting of continuous process of molecular motion and collisions into two successive stages at the time step Δt. The computational domain is divided into cells of size Δx such that the variation of the flow parameters in every cell is small. The time step Δt should be small as compared with the mean collision time τ_λ. Free motion of molecules and their collisions are considered successively at this time step Δt:

1. Collisions of particles belonging to the given cell in each cell of are carried out independently in each cell of physical space, i.e. the collisions of particles in the neighboring cells are not considered. Since the distribution function variation is supposed small in the cell, when a pair of particles for collision is chosen the relative distance between them is not taken into account. The post-collision velocities are calculated in accordance with the conservation laws of linear momentum and energy.

2. All molecules located in the computational domain are displaced by the distance determined by their velocities at the moment and by the time step Δt. If a molecule leaves the computational domain, then its velocity is recomputed according to the boundary conditions. At the same step Δt new particles entering the computational domain are generated in accordance with the distribution function specified at the domain boundaries.

Thus, the following principals steps are specified in the DSMC procedure:

- entering new molecules

- molecular motion
- gas/surface collisions
- indexing of molecules over collision cells
- collisions
- sampling of macroparameters

After finishing computation, the results of computations are processed to obtain the flowfields of gas dynamics parameters, total and distributed surface quantities. The main steps of the DSMC technique are discussed below.

The state of each simulated particle is characterized by its coordinate $\bar{r}$ and velocity $\bar{v}$. The state of the whole system of N particles is described by a $6N$-dimensional vector $\{\bar{R}, \bar{V}\} = \{\bar{r}_1, \bar{v}_1, ..., \bar{r}_N, \bar{v}_N\}$. The evolution of such a system can be represented as a jump-like motion of a point in the $6N$-dimensional phase space. The DSMC method can be then treated as statistical simulation of the $6N$-dimensional random jump-like process.

In the traditional approach Bird [1] of constructing numerical schemes of the DSMC method, the description of procedures for trajectory simulation of the random process is based on physical concepts of rarefied gas and on physical assumptions that create the basis for the phenomenological derivation of the Boltzmann equation.

A different approach was proposed by Ivanov and Rogasinsky [2] who constructed numerical schemes for simulating a $6N$-dimensional, continuous in time, random process of spatially nonuniform evolution of a system of N particles. Majorant collision frequency (MCF) schemes of the DSMC method were derived from the Kac [3] and Leontovich [4] master kinetic equations (MKE). This is a linear integro-differential equation that describes the time behavior of an N-particle gas model with binary collisions on the level of the N-particle distribution function f_N. The linear MKE may be transformed into the nonlinear Boltzmann equation when $N \to \infty$ and the molecular chaos condition is satisfied (see, e.g., [5]). Since a finite number of simulated particles is used in the DSMC simulations, it is natural to directly use MKE for constructing numerical schemes of the DSMC method. The procedure of constructing MCF schemes is described in detail in Appendix 1.

The extension of the majorant collision frequency schemes obtained from MKE to the case of multispecies chemically reacting mixtures is straightforward. It implies the change in cross-sections of the corresponding inelastic processes and, hence, the change in the collision algorithm only in the part that is related to the collision mechanics.

The procedures of modeling gas-surface interaction for two reflection models (specular-diffuse and Nocilla models) can be found in Appendix 2.

Currently used numerical schemes of the DSMC method (NTC [1], NCT [6], MCF [2, 7]) are very close both in terms of efficiency and numerical implementation. At present, there are no essential internal resources for increasing the efficiency of the collision stage of the DSMC method. The main effort in improving the method efficiency is directed to the study of influence of the grid type, the use of multi-zone approaches, variable time step, grid adaption procedures, etc [8,9,38].

3 Real gas effect models for DSMC

An accurate prediction of high-temperature rarefied flows, such as those behind the shock wave formed about a space vehicle at high altitudes, requires the use of adequate models of physical and chemical processes - so-called real gas effects, and effective numerical procedures. An example of the impact of these processes on the flow is given in Fig. 1 where the translational temperature fields about the Soyuz capsule at an altitude of 85 km are shown for nonreacting and reacting gases [9].

Two most important effects of chemical reactions are the decrease in temperature in the shock front and a smaller shock stand-off distance. In conventional continuum gas

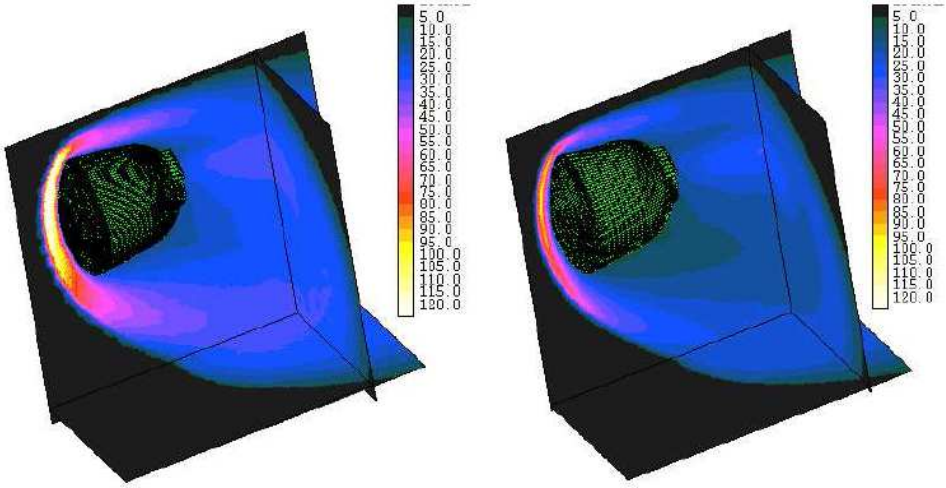

Figure 1: Translational temperature fields about a reentry capsule, altitude 85 km, velocity 8 km/s. Nonreacting (left) and reacting (right) air.

dynamics the real gas effects are usually understood as such high-temperature phenomena as molecular vibration, dissociation, ionization, surface chemical reactions, and radiation. In describing the problems of rarefied gas dynamics, with a typical large, often of the order of the reference flow scale, shock wave width and rarefaction effects exerting the determining effect on the flow structure, it is convenient to consider the "real gas effects" in a wider sense. As applied to kinetic methods based on the microscopic approach and used for studying RGD problems, it seems natural to relate the real gas effects with all phenomena associated with molecular collisions, namely, molecular interaction potential, rotational degrees of freedom, vibrational degrees of freedom, chemical reactions in gas, ionization, and radiation.

One of the most challenging problems remaining in terms of the method development and improvement is related to the need to effectively and reliably simulate processes of energy transfer between internal and translational modes, chemical reactions, ionization, and radiation. The presence of one or more of these processes drastically changes flow properties such as density and temperature, and the development of adequate models is therefore very important. A number of DSMC techniques and models were suggested

and used in the last decade that cover different aspects of the problem (see, for example, Refs. [10]-[14] and references therein). Currently, there is a lack of models that are general enough to treat various molecular interactions and processes, sufficiently accurate to capture complex flow physics, easy to implement, and computationally efficient to be applied to calculate near-continuum flows.

In what follows we would like to mention the collision models that are both computationally efficient, easy to implement, and sufficiently general to be applied for any type of interactions between atoms and diatomic and polyatomic molecules. The Variable Soft Sphere (VSS) model [15] is one of the most widely used models of intermolecular interaction. In this model the total collision cross-section depends on the relative collision velocity, and two parameters of the model are determined from the condition of coincidence of diffusion and viscous cross-sections of the VSS and the inverse-power potential models. Even though the model does not include the attractive part of the potential, it is applicable for most conditions where the DSMC is used. Rotational energy distribution is conventionally assumed to be continuous, which makes the energy transfer algorithms simpler, especially for polyatomic molecules.

The discrete description was suggested in [16] for different types of polyatomic molecules. The traditional Larsen-Borgnakke (LB) model [17] is most widely used in the DSMC method to describe the energy exchange between the translational and rotational modes of colliding particles. In this model, the energy spectrum of rotational mode is assumed continuous, and some fraction $\varphi = 1/Z_R$ of the total number of collisions takes place with the energy exchange between translational and rotational degrees of freedom. The post-collision rotational and relative translational energies are simulated in accordance with the local equilibrium distribution functions and are proportional to the number of degrees of freedom of the mode. Several improvements were suggested for the LB model to make the rotational relaxation rate in the DSMC modeling correspond to the continuum and experimental rates. First, temperature-dependent rotational collision number was suggested [12]. Then, a correction factor was derived that establishes a relation of Z_R employed in the DSMC method with a continuum analog used in the Jeans relaxation equation [18]. Finally, a particle selection methodology was proposed [19], which prohibits multiple relaxation events during a single collision, and matches Jeans equation for general gas mixtures. In contrast to the traditional LB model, the particle selection methodology prohibiting multiple relaxation events does not include directly rotational-rotational energy transfer. Note that this type of energy transfer has not been studied separately in the DSMC method. Since the translational-rotational energy transfer is fast, and rotational distribution is usually less important for chemical reactions and radiative processes than vibrational distribution, accurate modeling of the translational-rotational energy transfer is sufficient for most cases.

The spacing between rotational energy levels is small, and the continuum model of rotational mode approximates well the discrete distribution [20]. It is therefore reasonable to use the continuum Larsen-Borgnakke model with the temperature-dependent relaxation number, the correction factor [18] and a selection methodology that prohibits multiple relaxation events. Two models for the vibrational energy distributions, continuous and discrete, are traditionally used in the DSMC method. Generally, the continuity of the vibrational energy mode may be a too rough allowance, since the vibrational spectrum of real molecules is characterized by large gaps between the neighboring energy levels. Be-

sides the physical reason, there are several numerical problems connected with the use of the continuum vibrational energy spectra. These are the need for special cut-off parameters for the LB model when the number of vibrational degrees of freedom is less than two, additional assumptions that have to be used in the LB collision energy transfer modeling, and an inaccurate shape of the internal energy distribution functions at equilibrium [20]. The last point is important for reactions whose cross-sections directly depend on vibrational states (such as vibrationally favored reactions). Also, internal energy distribution strongly affects the flow radiation. The discrete internal energy model does not have these drawbacks, but requires a special correction procedure to be used for the chemical reaction rates to follow the experimental rates expressed in the Arrhenius form. Many discrete models for the translation-vibration energy transfer were suggested in the literature. They differ considerably in the way of determining the vibrationally inelastic cross-sections. A discrete version of the LB model is presented in [21]. In the model [22], the probability of VT transitions is determined using the inverse Laplace transformation for a simple harmonic oscillator from the temperature-dependent relaxation rate [23]. The approach [24] is based on the use of the information theory for determining post-collision states. In the model [25] the cross-sections for vibration-translation transitions are used, obtained for an anharmonic oscillator from a quasi-classical approximation of the scattering theory.

The vibration-vibration energy transfer was also modeled in the DSMC method. We mention here the model [26] where both vibration-translation and vibration-vibration transitions for a simple harmonic oscillator have been considered. The vibration-vibration energy exchange model based on the quasiclassical approach was developed in [25]. This energy transfer process was found to be important for the vibrational populations in hypersonic flows at high altitudes. All these and many other models have been developed only for diatomic molecules. Because of this, it seems most reasonable at present to use the LB model with particle selection. Temperature-dependent vibrational relaxation rate has to be specified using vibrational mode characteristic temperatures of polyatomic molecules. A correction factor [27] has to be used that enables one to match the vibrational relaxation rates in the DSMC modeling to the relaxation rate given by the Landau-Teller equation. Note that the LB model was not yet applied to vibration-vibration energy transfer. Such an application would require to specify the corresponding collision numbers that may not be known for many molecular systems.

The DSMC method has been used for calculating rarefied hypersonic chemically reacting flows for more than two decades. The major problem in generating the model of chemical reactions is the determination of energy-dependent cross-sections of chemical reactions. Note here that the temperature dependences of chemical reaction rates, traditional for the continuum approach, cannot be applied to the DSMC method, and energy-dependent reaction cross-sections have to be used. As the exact expressions for these cross-sections are not available now even for simple dissociation reactions in air, some approximations have to be employed. The first simplistic models have been replaced by the total collision energy (TCE) model [28] built on the basis of collision theory for chemical reactions. This model is efficient and is used presently for calculating two- and three-dimensional flows. It employs the major assumption that the reaction probability depends on the total collision energy. A specific form of this dependence is assumed that allows analytic determination of unknown coefficients. The derivation uses the reaction rate coefficient in Arrhenius form and the Hinshelwood expression for the equilibrium en-

ergy distribution function that implies continuous distribution of internal modes [28]. The problems inherent in continuous vibrational energy models that were discussed above lead to the conclusion that the use of discrete models in the DSMC method is preferable. One problem related to the use of discrete energy levels is that the existing chemical reaction models derived for continuous internal energies need special modifications to be applied for discrete energies. In this case, a correction procedure is necessary for the reaction rates in the DSMC method match available experimental data. Such a correction procedure was developed in [20]. It utilizes a Monte Carlo approach to find modified constants in the reaction cross-section energy dependence, the use of which enables one to match the original reaction rates at equilibrium.

The procedure is applied to the total collision energy model, but is generally applicable to any reaction model based on the collision theory for chemical reactions. Several models that include a direct dependence of the reaction cross-sections on the collider vibrational energy (so-called vibration-dissociation coupling) were proposed earlier [10, 13, 14]. The deficiency of these models is that they imply some fixed or variable parameters that determine the extent of vibrational favoring. These parameters are extracted or verified through comparison with available experimental data. Note that some reactions may not have vibrational favoring, and therefore the model [28] may turn to be reasonable [29].

4 DSMC versus continuum CFD

The areas where the continuum and kinetic approaches are currently applied overlap in the regime of low Knudsen numbers. The recent experimental and computational activity related to accurate prediction of laminar flow separation in the near-continuum regime shows that even for non-reacting gases there are still problems of validation and verification of numerical approaches that need to be resolved. Numerical analysis of such flows is traditionally performed using Navier-Stokes (NS) equations, with the initial effects of rarefaction taken into account through the slip velocity and temperature jump. The use of slip conditions is caused by the fact that rarefaction effects can be observed for slender bodies even for rather high Reynolds numbers ($Re = 20,000 - 30,000$). The state-of-the-art algorithms of the DSMC method (adaptive grids, variable time step, etc.) allow one to simulate flows at such high Reynolds numbers. This makes realistic the study of the applicability area of the continuum approach to model laminar separated flows. The study was started in [30] and continued in [31] where a detailed numerical modeling of an axisymmetric shock wave / laminar boundary layer interaction was performed by the continuum (NS) and kinetic (DSMC) approaches for the ONERA R5Ch wind tunnel conditions. The DSMC results showed the presence of a high slip velocity and temperature jump near the wall. The application of slip conditions for the NS solver has a substantial effect on the entire flow field and allows one to decrease the difference between the continuum and DSMC results. The left part of Fig. 2 shows that the profile of the gas velocity at the wall U_g obtained by the DSMC method is in excellent agreement with the U_g profile calculated from the NS slip velocity using the solution for the velocity distribution across the Knudsen layer [32]. However, the NS solver with slip conditions predicts a larger length of the separation region than the DSMC method. To eliminate

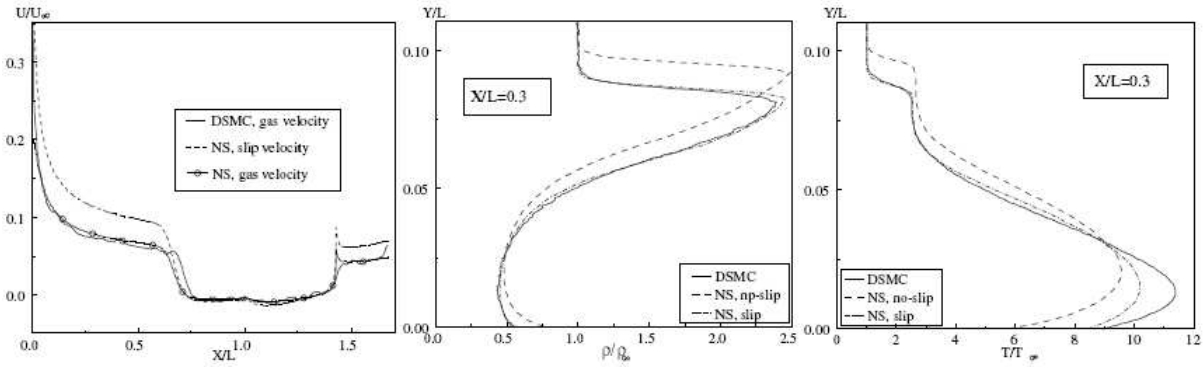

Figure 2: Slip and gas NS velocities and gas DSMC velocity at the wall (left). Density (center) and temperature (right) profiles for a monatomic gas.

the effect caused by different descriptions of translational/rotational energy exchange for both methods, NS and DSMC simulations of a laminar separated flow of a monatomic gas (argon, $M = 10$) were performed in [32]. The central part of Fig. 2 shows the comparison of density profiles in the cross-section $X/L = 0.3$. The use of slip conditions for the NS solver reduces the slope of the leading-edge shock wave and generally gives a good agreement with the DSMC results. The comparison of temperature profiles (right part of Fig. 2) shows that the difference between the no-slip continuum and kinetic results reaches 40%. The use of the slip conditions allows one to obtain the temperature near the body surface that is very close to the DSMC values, and also decrease the difference inside the boundary layer. Still, the temperatures inside the boundary layer for DSMC and NS with slip conditions differ by about 20%. Figure 3 shows the distributed aerothermodynamic

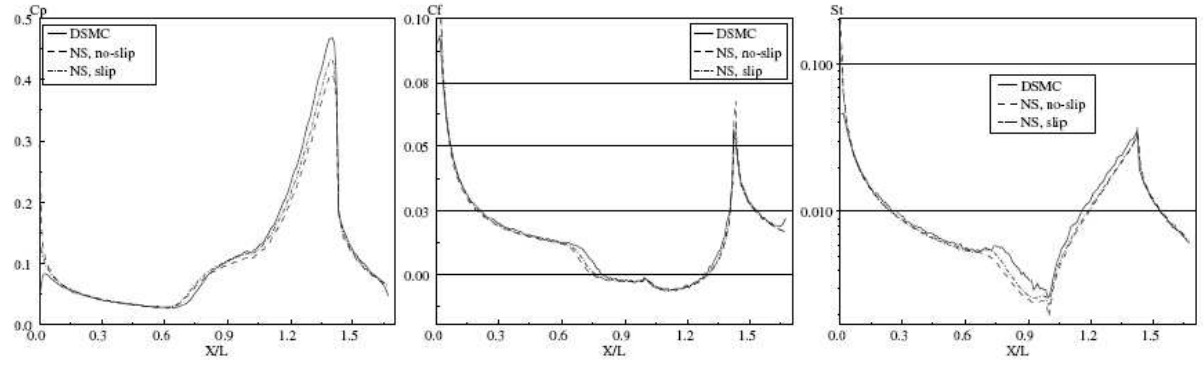

Figure 3: Distributed surface characteristics for monatomic gas. Pressure coefficient (left), skin friction coefficient (center), and Stanton number (right)

characteristics obtained using the continuum and kinetic approaches. The differences in the pressure and skin friction coefficients and the Stanton number are mainly due to the following two factors. First, the length of the separation region is different. An earlier flow separation in NS results leads to a lower pressure peak and smaller heat flux on the flare surface. Second, there is a strong flow nonequilibrium near the leading edge. This is why the NS solver with either no-slip or slip conditions predicts a significantly larger

heat flux (up to a factor of four) than the DSMC method in the vicinity of the leading edge. This also leads to a significant decrease in the flow temperature downstream and an earlier separation of the boundary layer. The studies conducted for a hypersonic flow around a hollow-cylinder flare clearly showed that the Navier-Stokes equations, even with slip conditions, are inapplicable in the vicinity of the leading edge. The flow near the leading edge affects the flow structure downstream, for example, leads to an increase in the separation region length.

5 Numerical accuracy of the DSMC method

An important problem that arises when modeling near-continuum flows is the evaluation of the numerical accuracy. Applying the DSMC method to compute transitional flows ($Kn \sim 1$), one can usually perform additional computations on a finer grid and with a larger number of simulated molecules in order to analyze the numerical accuracy. For a near-continuum regime, the computations are often conducted using all available computer resources, and no additional accuracy-establishing computations are possible in this case. The question is therefore what is the accuracy of results obtained, and how far they are from the solution of the Boltzmann equation. This question is especially important for the near-continuum flows.

The sources of numerical error have been analyzed in the continuum CFD for many years. There are many techniques available such as the analysis of truncation errors, the grid convergence study, etc., that enable one to estimate the accuracy of the results. There is nothing similar for the DSMC method. The accuracy analysis in DSMC is complicated by the presence of different errors that may be classified as follows: (1) statistical errors; (2) spatial resolution and time step errors; (3) errors due to the finite number of simulated molecules. The complete analysis of the accuracy should include the derivation of the governing equation that describes the modeling process, and establishing of the connection between this equation and the Boltzmann equation. This connection can hardly be established for the NTC and NCT schemes because these schemes were formulated at the phenomenological level.

The MFS scheme was derived from MKE, which describes the behavior of an N-particle gas model with binary collisions. This equation may be transformed to the Boltzmann equation when $N \to \infty$ and the molecular chaos condition is satisfied. Let us examine the molecular chaos requirement in more detail. A finite number of molecules N is always used in DSMC modeling. Therefore, there is a statistical dependence between simulated particles [33]. The magnitude of this dependence depends on the total number of simulated molecules in the system, and generally decreases when the number of molecules increases. It is necessary to estimate the level of statistical dependence and its contribution to the results of DSMC computation. A significant level of statistical dependence, or particle correlations, means that the molecular chaos hypothesis, used in the Boltzmann equation, is no longer valid. The molecular chaos hypothesis may be written in terms of one- and two-particle distribution functions, f_1 and f_2 , as

$$f_2(\nu_A, \nu_B) = f_1(\nu_A) f_1(\nu_B),$$

where ν_A and ν_B are the velocities of the two collision partners, A and B. For some function of velocity, $h \equiv h(\nu)$, we can write

$$\int_{-\infty}^{\infty} f_2(\nu_A, \nu_B) h(\nu_A) h(\nu_B) d\nu_A d\nu_B = \int_{-\infty}^{\infty} f_1(\nu_A) h(\nu_A) d\nu_A \int_{-\infty}^{\infty} f_1(\nu_B) h(\nu_B) d\nu_B$$

This expression may be rewritten as

$$\langle h(\nu_A) h(\nu_B) \rangle = \langle h(\nu_A) \rangle \langle h(\nu_B) \rangle$$

where $\langle ... \rangle$ denotes averaging. As was mentioned above, the molecular chaos hypothesis is not strictly valid for a finite number of particles, which means that the above expression does not hold. Let us introduce the following correlator G_2,

$$G_2 = \frac{\langle h(\nu_A) h(\nu_B) \rangle}{\langle h(\nu_A) \rangle \langle h(\nu_B) \rangle} - 1$$

Obviously, this correlator may serve as an indicator of the presence of molecular correlations. The smaller the correlations, the closer G_2 is to 0. The value of G_2 may be directly calculated in the DSMC method over all cells in the computational domain, and $h(\nu) = V_x^2$ is usually used for this purpose [34], [35]. An additional criterion that allows for a practical verification of the presence of the statistical dependence between simulated particles is the relative number of repeated collisions [34]. Repeated collisions are collisions between the same pair of particles during their lifetime in the computational domain. The number of repeated collisions is directly related to the number of particles N_λ in a volume with the linear size equal to the local mean free path. If $N_\lambda > 1$, one can say that the simulation results are close to the solution of the Boltzmann equation. Let

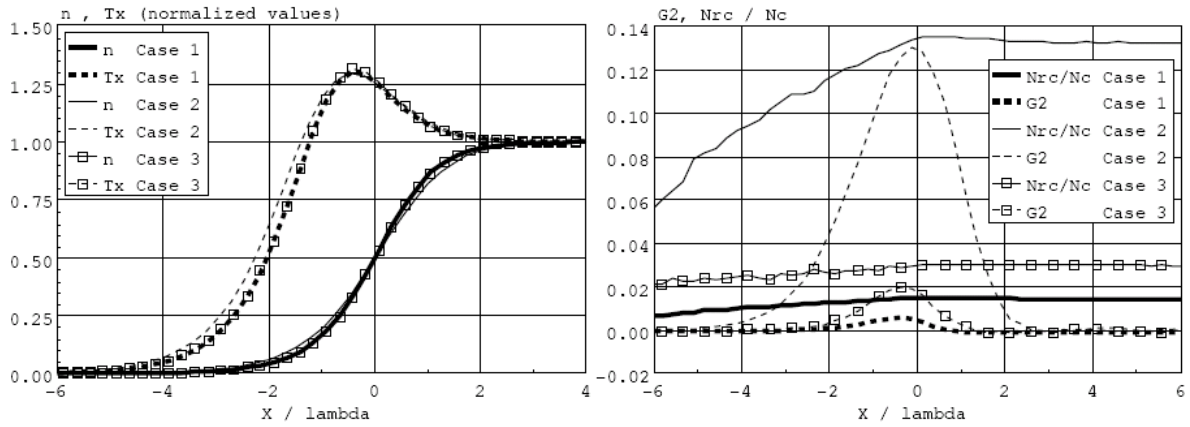

Figure 4: $1D$ shock wave, monatomic gas. Density n and parallel temperature T_x (left). Correlator $G^2(V_x^2)$ and repeated collision fraction (right).

us consider a $1D$ shock wave structure as an example where the G_2 correlator and the repeated collision number are used. A monatomic gas of hard sphere molecules is used with $M = 8$. The computational domain was 15 upstream mean free paths. Three cases were considered here. 20 particles in the upstream cells was used in Case 1 (baseline case),

with the cell size L of 0.25 of the upstream mean free path λ. For Case 2, 2 particles per upstream cell was used with $L = 0.25\lambda$. The number of particles for case 3 was the same as in Case 1, but $L = 0.00625\lambda$. The average number of particles in the upstream cells was therefore 0.5 in this case.

The density and parallel temperature distributions inside the shock wave are shown in Fig. 4 (left). The profiles are very similar for Cases 1 and 3, and somewhat different for Case 2. The G_2 correlator and repeated collision fraction are given in Fig. 4 (right). For Case 1, the values of G_2 are close to zero, being less than 0.01 even in the region of strong nonequilibrium, and the number of repeated collisions is not greater than 2 percent of the total number of collisions. The values of the correlator and repeated collision fraction increase about ten times for Case 2 compared to case 1, even though the collision frequency is the same since the MFS scheme is used. The increase in the particle statistical correlations is the reason for the difference in the macroparameters observed in Fig. 4 (left). Obviously, the difference is due to the decrease in the total number of simulated particles in the computational domain. We can therefore state that an accurate calculation of the collision frequency in a cell is not sufficient for obtaining an accurate result. An interesting fact is that the reduction of the cell size while preserving the total number of molecules (Cases 1 and 3) does not change macroparameters and only slightly changes the correlator and the number of repeated collisions. This shows that the number of particles in cell is not a determining factor for MFS. The important parameters are the total number of particles in the system and N_λ.

This fact is illustrated below for a flow over a cylinder in CO_2/N_2 mixture [36]. A free-stream velocity of 7400 m/s, temperature of 137.4 K and Knudsen number $Kn = 0.01$ were taken. The mole fractions of CO_2 and N_2 were assumed to be 0.9537 and 0.0463, respectively. A diffuse reflection with complete energy accommodation was employed at the surface with temperature value of 1000 K. The computations were performed for different numbers of simulated molecules in the computational domain in order to examine the impact of N_λ on results. An adaptive grid refinement technique was used to satisfy the $Kn_c > 1$ condition in the entire computational domain. The profiles of translational and vibrational temperatures along the stagnation line are plotted in Fig. 5 ($X = 0$ corresponds to the stagnation point). The results are shown for different values of N_λ in the free stream which corresponds to different values of the total number of simulated particles. The N_λ distribution along the stagnation line is also presented here. The local N_λ is not less than 1 for the free stream $N_\lambda = 20$, and this case is therefore considered to be the reference. It is seen that for $N_\lambda = 2.5$ in the free stream the results agree with the reference case inside the shock wave, but are somewhat different near the stagnation point. This is because N_λ in this region decreases sharply and becomes less than 1. When the free stream N_λ is further decreased, the results are relatively close to the reference case inside the shock, but significantly differ inside the boundary layer. It should be noted that the impact of N_λ is more pronounced for the vibrational temperature than for the translational one. The results presented show that the condition $N_\lambda > 1$ must be satisfied in DSMC simulations for the impact of particle correlations be insignificant.

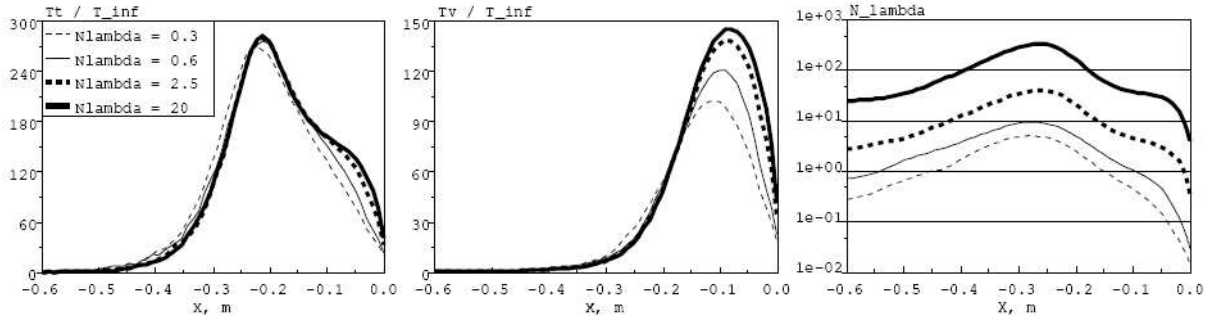

Figure 5: Translational T_t (left) and vibrational T_v (center) temperatures and N_λ (right) along the stagnation line for different free stream N_λ values.

6 High-altitude aerothermodynamics of a promising capsule

PPTS (Prospective Piloted Transport System), unofficially called Rus, is a project being undertaken by the Russian Federal Space Agency to develop a new-generation manned spacecraft. Its official name is Pilotiruemyi Transportny Korabl Novogo Pokoleniya or PTK NP meaning New Generation Piloted Transport Ship. The goal of the project is to develop a new-generation spacecraft to replace the aging Soyuz which was developed by the former Soviet Union more than forty years ago.

At the initial stage of spacecraft design, it is necessary to study its aerothermodynamic characteristics in a wide range of free-stream parameters. During de-orbiting, the vehicle passes through the free-molecular flow, then through the transitional zone, and the flight is finalized in the continuum flow. The loads on the vehicle during its descent are considerably changing. The efficiency of control surfaces is also changing. To predict the zone of spacecraft landing, one should know the aerodynamic characteristics of the vehicle at all stages of its descent. The results of statistical simulation of aerothermodynamics of a promising space capsule at altitudes from 120 to 60 km are presented below (for details, see [47]).

The aerothermodynamic parameters of the space vehicle at altitudes from 120 to 60 km were studied by the local bridging method. Standard atmosphere parameters were taken for computations from GOST 4401-81. The DSMC method was used to model the flow at several altitudes with the parameters listed in Table 1.

H, km	75	80	85	90	100	110
M_∞	25.9	26.5	27.2	27.3	26.3	22.5
T_∞, K	208.4	198.6	189.0	186.7	196.6	255.5
ρ_∞, kg/m^3 $\cdot 10^6$	39.9	18.5	8.21	3.42	0.56	0.093
Kn_∞	$0.38 \cdot 10^{-3}$	$0.8 \cdot 10^{-3}$	$0.18 \cdot 10^{-2}$	$0.43 \cdot 10^{-2}$	$0.27 \cdot 10^{-1}$	0.17

Table 1: Parameters of the atmosphere (GOST 4401-81)

The space vehicle considered is shaped similar to the Apollo capsule. The nose part is

spherical, and the rear part is beveled at an angle of 20°. The vehicle geometry is shown in Fig. 6. A qualitative difference from the Apollo capsule is the presence of trimming flaps. One of the objectives of the present activities was to determine the changes in efficiency of these flaps with variations of the angle of attack and with allowance for real gas effects. The temperature of the entire body was assumed to be constant and equal to 1000 K.

The influence of chemical reactions proceeding in the flow on the efficiency of control surfaces was determined in an axisymmetric formulation. As the axisymmetric formulation allows us to obtain the aerodynamic characteristics of only those elements that are obtained by means of rotation by 360°, but the trimming flaps have finite size, their contribution to the aerodynamic parameters was taken into account with the following procedure: the aerodynamic loads (C_X and C_Y) on a circular flap were identified; then the fraction of the loads on the flap in accordance with its angular size was calculated; finally, the pitching moment generated by the flaps was found from the loads obtained ($C_{X\,flap}$ and $C_{Y\,flap}$).

The DSMC computations were performed with the use of the SMILE software system [7]. The internal energy exchange was modeled in accordance with the Larsen–Borgnakke model. Chemical reactions that occur during particle collisions were also taken into account. Diffuse reflection from the surface with complete accommodation of energy was assumed.

The computations were performed on clusters of the Interdepartmental Supercomputer Center (Moscow, Russia) and of the Khristianovich Institute of Theoretical and Applied Mechanics of the Siberian Branch of the Russian Academy of Sciences (Novosibirsk, Russia). Up to 128 processors were used. The computations at an altitude of 75 km required approximately 7000 processor-hours.

The local bridging method used in this work is based on the technique proposed in [46]. The influence of the flow on an elementary area is described by the following formulas:

$$P = P_0 + P_1 w_n + P_2 w_n^2 \qquad \tau = \tau_0 w_t + \tau_1 w_n w_t \tag{1}$$

Here P and τ are the pressure and friction coefficients of aerodynamic forces normalized to the dynamic pressure $q = \frac{\rho_\infty V_\infty^2}{2}$, $\vec{w}$ is the normalized free-stream velocity vector, and w_n and w_t are the normal and tangential components of the velocity vector to the surface. The parameters P_0, P_1, P_2, τ_0, and τ_1 are calculated using the following formulas:

$$P_0 = P_0^{id} + (P_0^{fm} - P_0^{id})F_{P0} \qquad P_1 = P_1^{fm} F_{P2} \qquad P_2 = P_2^{id} + (P_2^{fm} - P_2^{id})F_{P2} \tag{2}$$

$$\tau_0 = \tau_0^{fm} F_{\tau 0} \qquad \tau_1 = \tau_1^{fm} F_{\tau 1} \tag{3}$$

($\vec{n}$ is the normal vector to the surface and $\vec{\tau}$ is the tangential vector). These vectors lie in one plane.

The bridging coefficients F_{P0}, F_{P1}, F_{P2}, $F_{\tau 1}$, and $F_{\tau 1}$ are used to take into account the influence of the free-molecular or continuum flow regime under particular conditions.

The formulas for calculating the bridging functions F_P and F_τ were derived semi-empirically in [46] Here we give their final form:

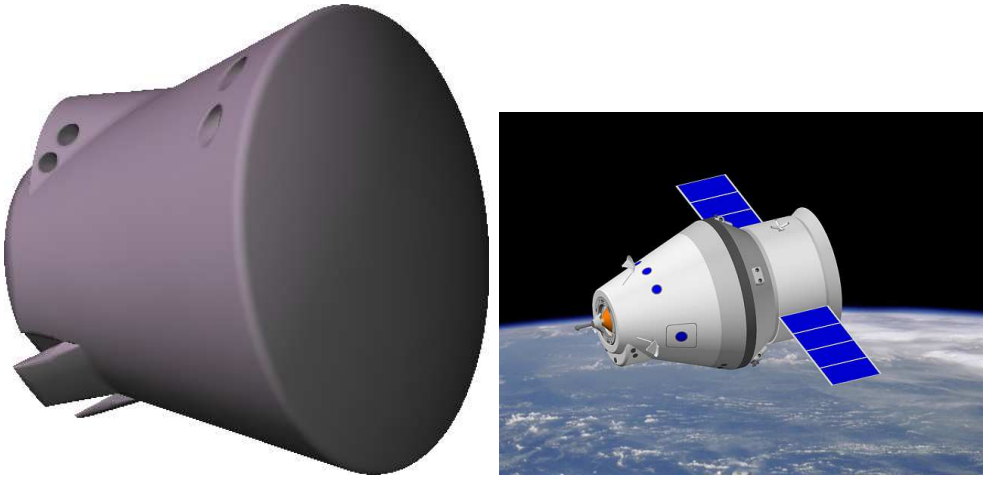

Figure 6: Space vehicle geometry

$$F_{P0} = \frac{1}{a\sqrt{\mathrm{Re}_0} + \exp(-b\mathrm{Re}_0)}, \qquad \text{where} \tag{4}$$

$$a = \frac{(\gamma-1)\sqrt{t_w} + \mathrm{M}^{-1}\sqrt{2(\gamma-1)}}{(0.56+1.2t_w)(\mathrm{M}+2.15)} \qquad b = 0.35 + 0.005\mathrm{M} \tag{5}$$

$$F_{P1} = F_{P2} \;=\; \exp\left(-(0.125+0.078t_w)\mathrm{Re}_0 \cdot 10^{-1.8(1-\sin\alpha_l)^2}\right) \tag{6}$$

$$F_{\tau 0} = \left[a_1\mathrm{Re}_0 + \exp(-b_1\mathrm{Re}_0)\right]^{-3/4}, \qquad \text{where} \tag{7}$$

$$a_1 = \frac{\gamma-1}{2}\left[\sqrt{\frac{\pi\gamma}{2}}\mathrm{M}(0.208+0.341t_w)\right]^{-3/4} \qquad b_1 = 0.213 - 0.133t_w \tag{8}$$

$$F_{\tau 1} = \left[0.145R + \exp\left(7.2\cdot 10^{-3}R - 1.6\cdot 10^{-5}R^2\right)\right]^{-1/2}, \qquad \text{where} \tag{9}$$

$$R = (0.75t_w + 0.25)^{-2/3}\,\mathrm{Re}_0 \cdot 10^{-2.4(1-\sin\alpha_l)^3} \tag{10}$$

Figure 7 shows the pressure fields calculated for non-deflected control flaps and for flaps deflected by 30°. The calculations were performed for a gas without chemical reactions. As it could be expected, the flap influence extends to a fairly small distance upstream, but the field in the wake behind the vehicle is noticeably changed. Thus, for instance, the pressure in the middle of the vehicle base area is approximately 90 Pa for the non-deflected flap and about 50 Pa for the flap deflected by 30°. In a hypersonic flow (M = 25.9), the base pressure does not exert any significant influence on the values of the total aerodynamic coefficients. Flap deflection increases the drag coefficient C_D from 1.50 to 1.54. The lift coefficient is $C_L = 0.103$ for the flap deflected by 30°.

The effect of chemical reactions on the flow field is illustrated in Fig. 8, which shows the pressure fields around the space vehicle obtained in a chemically reacting flow (upper

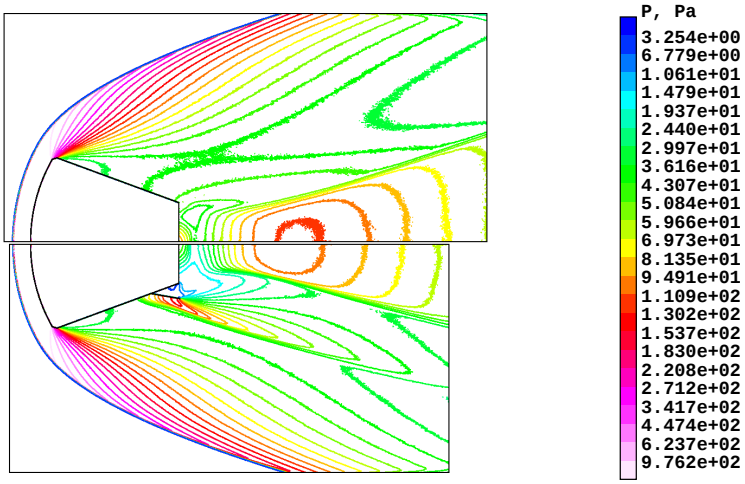

Figure 7: Pressure fields. Altitude 75 km. Chemically inert gas. Non-deflected flap (upper) and flap deflected by 30°(downer).

figure) and in a chemically inert gas (lower figure) for the flap deflected by 30°. The calculations were performed for an altitude of 75 km. It is seen that the flow fields are drastically different in the entire computational domain. Indeed, as the major part of the free-stream energy is spent on dissociation of diatomic molecules, the flow temperature in the case of a chemically reacting gas is substantially lower than the temperature obtained with the chemical reactions being ignored. In addition to temperature fields, the Mach number fields are also essentially different. Therefore, we can conclude that the entire flow structure and the shock waves near the vehicle are formed in a different manner.

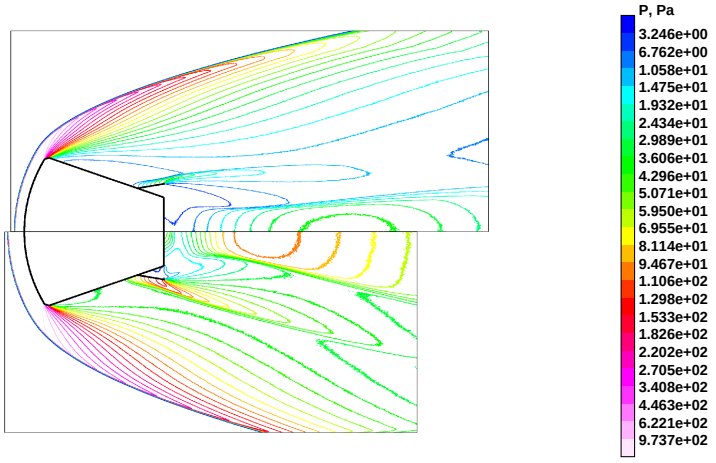

Figure 8: Pressure fields. Altitude 75 km. Flap deflection angle 30°. Chemically reacting gas (upper figure) and chemically inert gas (lower figure).

Figure 9 shows the distributions of temperature and pressure normalized to the free-stream pressure over the stagnation lines at altitudes of 75, 85, and 90 km. The plots show the stagnation lines obtained for chemically reacting and chemically inert gases. The plots on the left show the free-stream parameters, and the plots on the right show the situation with the body located at $X = 0$. It is seen that the temperature of the flow behind the bow shock wave is substantially lower if chemical reactions are taken

into account. In addition, the stand-off distance of the bow shock wave is changed. The influence of chemical reactions becomes attenuated with increasing flight altitude. Thus, for instance, the difference in the shock-wave stand-off distance is 0.187 m at an altitude of 75 km, 0.133 m at 85 km, and 0.093 m at 90 km.

At altitudes from 75 to 90 km, the space vehicle moves in the flow regime close to continuum (the Knudsen number changes from $3.7 \cdot 0^{-4}$ to $4.3 \cdot 10^{-3}$). The drag coefficient C_D at altitudes from 75 to 90 km is almost independent of the flight altitude and the presence of chemical reactions; its value is approximately 1.55. The heat-transfer coefficients $C_h = \frac{Q}{\frac{\rho_\infty V^3}{2} S_*}$ obtained in computations with and without chemical reactions are listed in Table 2. It is seen from the Table that the heat-transfer coefficient decreases by more than a factor of 3 at an altitude of 75 km and by a factor of 2 at an altitude of 90 km if chemical reactions are taken into account.

To determine the efficiency of control surfaces, we performed three-dimensional computations of spacecraft aerodynamics with the flap deflected by 0, 20°, and 30°at altitudes from 80 to 110 km for angles of attack 0 and 40°. As an example, Fig. 10 shows the pressure field and the surface distribution of the pressure coefficient at an altitude of 80 km at a zero angle of attack and 40°. It is seen from these figures that the control flap induces an extremely weak perturbation into the flow at a zero angle of attack, but its influence on the flow field becomes fairly significant as the angle of attack is increased to 40°.

The DSMC method is too expensive to perform a multiparametric study of aerothermodynamic characteristics of the space vehicle at different angles of attack, different altitudes, and different angles of flap deflection.

For this reason, another series of computations was performed by the engineering local bridging method. To estimate their accuracy, the results of these computations were compared with the DSMC results. Figure 11 shows the aerodynamic characteristics as functions of the angle of attack for a flap deflection angle of 30°. The curves show the results for the angle of attack equal to 0 (1), 10 (2), 20 (3), 30 (4), and 40°(5). Dahsed curves 6 and 7 show the results of the 3D DSMC computations for the angles of attack equal to 40°and 0, respectively. There is no curve that refers to the zero angle of attack in the $C_N(H)$ plot, because the normal force is close to zero at the zero angle of attack.

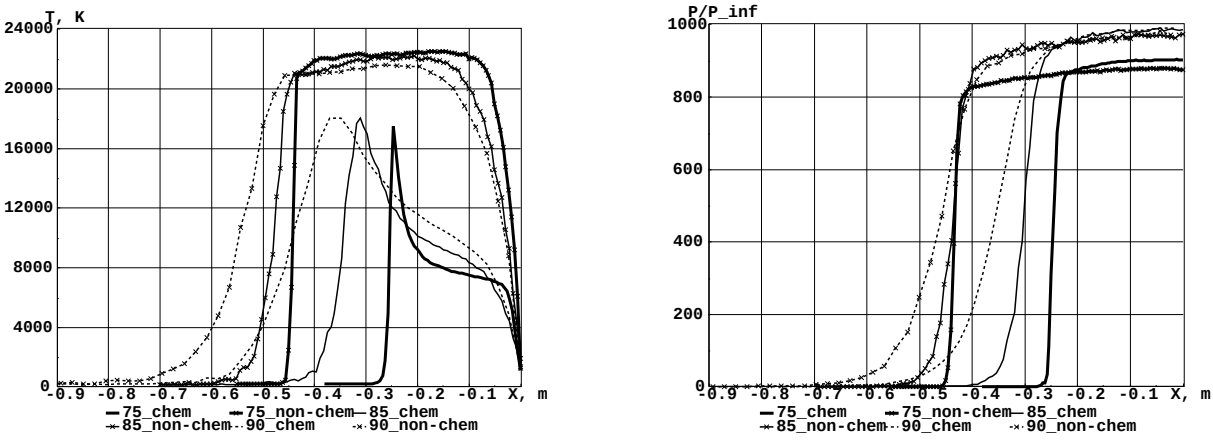

Figure 9: Overall temperature (left) and pressure (right) along the stagnation line at different altitudes. Axisymmetric computation.

Altitude, km	75	80	85	90
Chemically reacting flow	$1.30 \cdot 10^{-2}$	$2.11 \cdot 10^{-2}$	$3.38 \cdot 10^{-2}$	$6.18 \cdot 10^{-2}$
Chemically inert flow	$4.30 \cdot 10^{-2}$	$6.22 \cdot 10^{-2}$	$9.47 \cdot 10^{-2}$	$1.36 \cdot 10^{-1}$

Table 2: Heat-transfer coefficient C_h of the vehicle. DSMC results. Non-deflected flaps. Axisymmetric model

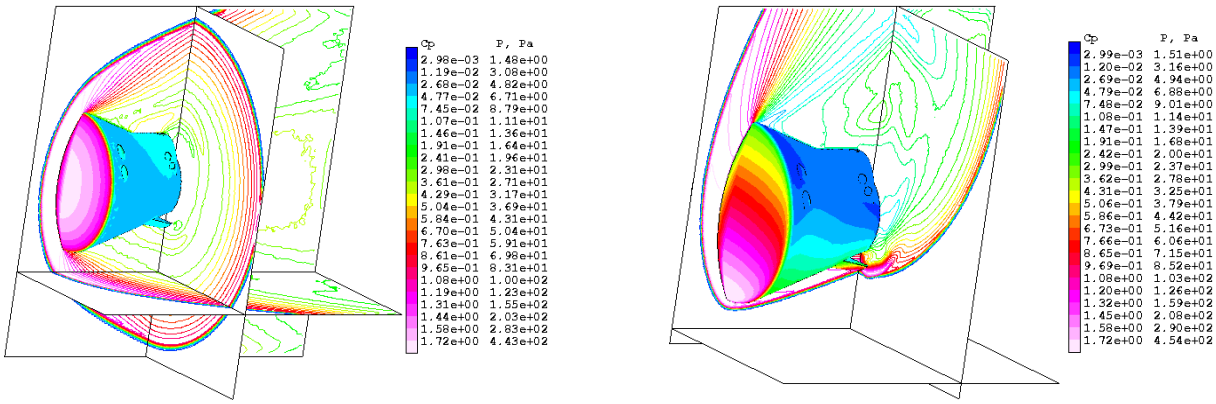

Figure 10: Pressure field and surface distribution of the pressure coefficient. Altitude 80 km. Flap deflection angle 30°. Angle of attack: 0 (left) and 40°(right)

The moment characteristic differs from zero, because the center of gravity is shifted down on 0.156 m from the spacecraft axis. The curves obtained by the engineering method describe the aerodynamic coefficients in the range of altitudes between 120 and 60 km. The difference from the DSMC results is approximately 5% for the force characteristics. The accuracy of the moment characteristics is lower, especially at an angle of attack of 40°at altitudes of 100 and 110 km (about 50%). It should be mentioned, however, that the value of the pitching moment coefficient is close to zero, and the large relative difference actually means insignificant absolute difference in the pitching moment coefficient. The DSMC computations reveal a significant effect of chemical reactions on the flow fields around the spacecraft and on the heat-transfer coefficient at altitudes below 90 km. Because of considerable changes in the flow structure near the base surface of the spacecraft,

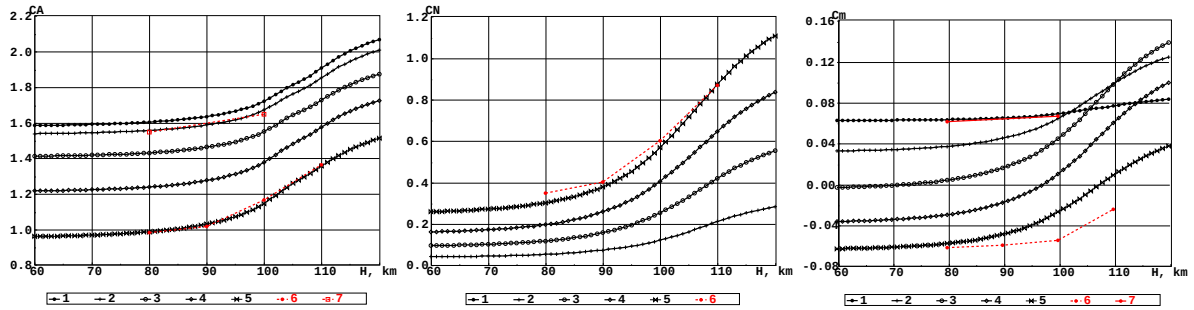

Figure 11: Axial and normal force coefficients and pitching moment coefficient versus altitude for different angles of attack. Flap deflection angle 30°. Angle of attack 0°(1), 10°(2), 20°(3), 30°(4), and 40°(5); DSMC results for the angle of attack equal to 40°(6) and 0°(7).

there is a several-fold difference in the values of the pitching moment and the lift force of the vehicle with deflected control surfaces, which were obtained with and without chemical reactions. Simultaneously, chemical reactions proceeding in the gas exert practically no effect on the drag coefficient. The changes in the aerodynamic characteristics with variations of the angle of attack and the angle of flap deflection at altitudes from 80 to 110 km were computed by the DSMC method. The aerodynamic characteristics of the spacecraft at altitudes from 120 to 60 km were also calculated by the engineering local bridging method. Comparisons with the DSMC results showed that the axial and normal force coefficients are calculated rather accurately (within 5%). The results obtained can be used to design the thermal protection system of the space vehicle and to construct its de-orbiting trajectory.

7 Prospects for the DSMC method

In conclusion, let us mention the directions for the DSMC method development that we believe will be important in the next several years.

- near-continuum flows: modeling of flows at relatively high Reynolds numbers (20,000 and higher) using both conventional DSMC method and computationally efficient hybrid approaches
- real gas effects: development of general models applicable for any type of molecules that would accurately predict the energy transfer processes and chemical reactions
- numerical accuracy check: use of available and development of new criteria that enable one to evaluate the numerical accuracy of results obtained, especially in the near-continuum regime
- extensive validation of models and algorithms: comparison of DSMC results with experimental data and contin- uum results in different gas dynamic situations for inert and reacting gases
- efficient parallel algorithms with dynamic load balancing: these are critical for modeling of computationally intensive two- and three-dimensional problems

8 Acknowledgments

The author would like to thank the research team of the Computational Aerodynamics Laboratory of the Institute of Theoretical and Applied Mechanics, Siberian Branch of the Russian Academy of Sciences. Our special thanks to Yevgeniy Bondar, Alexander Kashkovsky, Dmitry Khotyanovsky, Alexei Kudryavtsev, Gennady Markelov, Alexander Shevyrin, Alina Alexeenko and Pavel Vashchenkov, who provided results of computations and participated in discussions and preparation of this paper. This work was supported by the Russian Foundation for Basic Research (Grant No. 10-08-01203-a).

A Appendix 1. Majorant collision frequency schemes

The DSMC method is traditionally considered as a method of statistical simulation of the behavior of a great number of model gas molecules. Usually the number of simulated particles is large enough ($\sim 10^5 - 10^8$), but this is extremely small in comparison with the number of molecules that would be present in the real gas flow. Each simulated particle is then regarded as representing an appropriate number of real molecules.

The state of each simulated particle is characterized by its coordinate $\bar{r}$ and velocity $\bar{v}$. The state of the whole system of N particles is described by the $6N$-dimensional vector $\{\bar{R}, \bar{V}\} = \{\bar{r}_1, \bar{v}_1, ..., \bar{r}_N, \bar{v}_N\}$. The evolution of such a system can be represented as a jump-like motion of a point in the $6N$-dimensional phase space. The DSMC method can be then treated as statistical simulation of the $6N$-dimensional random jump-like process. For such a simulation, it is necessary to generate the trajectory of the random process. To this end, it is needed to determine a technique for simulation of the initial trajectory point of the random process $(t_0, \bar{R}_0, \bar{V}_0)$, transition in time between subsequent collisions (free motion) from the state $(t_0, \bar{R}_0, \bar{V}_0)$ to the state $(t_1, \bar{R}_1, \bar{V}_0)$, and the changes in particle velocities after collisions, i.e. the transition from the state $(t_1, \bar{R}_1, \bar{V}_0)$ to $(t_1, \bar{R}_1, \bar{V}_1)$. Then transitions from state 1 to state 2, etc. are considered. The trajectory is terminated when $t_n > T$ where T is the modeling time.

In the traditional approach of constructing numerical schemes of the DSMC method [1], the description of procedures for trajectory simulation of the random process is based on physical concepts of rarefied gas and on physical assumptions that form the basis for the phenomenological derivation of the Boltzmann equation.

The kinetic theory of gases makes use of the so-called "master" kinetic equations (MKE) [3,4] which describe the behavior of an N-particle gas model with binary collisions. These linear MKE transform to the nonlinear Boltzmann equation when $N \to \infty$ and molecular chaos conditions are satisfied (see, e.g., [5]). Since a finite number of simulated particles is used in numerical simulation, it is natural to utilize directly these MKE equations for constructing numerical schemes of the DSMC method. Such an approach to the derivation of numerical schemes of the DSMC method was presented in [2,33,37].

First, let us consider a spatially-uniform rarefied gas flow, and present the main steps of constructing numerical schemes directly from the MKE. In this case, it is possible to use the Kac master equation [3]:

$$\frac{\partial}{\partial t} f_N(t, \bar{V}) = \frac{n}{N} \sum_{i<j} \int_0^{2\pi} d\epsilon_{ij} \int_0^{\infty} b_{ij} db_{ij} |\bar{v}_i - \bar{v}_j| \{ f_N(t, \bar{V}'_{ij}) - f_N(t, \bar{V}) \}, \qquad (1)$$

where $\bar{V} = (\bar{v}_1, \ldots, \bar{v}_N)$ is a $3N$-dimensional vector of particle velocities; $\bar{V}'_{ij} = (\bar{v}_1, \ldots, \bar{v}'_i, \ldots, \bar{v}'_j, \ldots, \bar{v}_N)$; b_{ij} and ϵ_{ij} are the impact parameters; $(\bar{v}'_i, \bar{v}'_j)$ and $(\bar{v}_i, \bar{v}_j)$ are the pre- and post-collisional velocities of i, j molecules, n is the number density, and the sum over $i < j$ means the summation over $N(N-1)/2$ collision pairs.

This is a linear integro-differential equation that describes the time behavior of the N-particle distribution function $f_N(t, \bar{V})$, $\int f_N(t, \bar{V}) d\bar{V} = 1$.

In accordance with the general theory of Monte Carlo methods [39,40], the following approach is used: the transition from an integro-differential form of the master kinetic

equation to a linear integral equation whose probability treatment serves as the basis for constructing an appropriate random process of direct simulation.

Using a function w – the probability density of transition of a pair of particles from $(\bar{v}_i', \bar{v}_j')$ to $(\bar{v}_i, \bar{v}_j)$, eqn (1) is written as

$$\frac{\partial}{\partial t} f_N(t, \bar{V}) + \nu(\bar{V}) f_N(t, \bar{V}) = \frac{n}{N} \sum_{i<j} \int f_N(t, \bar{V}_{ij}') w(\bar{v}_i', \bar{v}_j' \to \bar{v}_i, \bar{v}_j) d\bar{v}_i' d\bar{v}_j', \tag{2}$$

where $\nu(\bar{V})$ is the total collision frequency

$$\nu(\bar{V}) = \frac{n}{N} \sum_{i<j} \int w(\bar{v}_i' \bar{v}_j' \to \bar{v}_i, \bar{v}_j) d\bar{v}_i' d\bar{v}_j' = \frac{n}{N} \sum_{l=j}^{N} \int \sigma\left(g_{ij}, \xi_{ij}\right) \delta_3\left(\bar{v}_i + \bar{v}_j - \bar{v}_i' - \bar{v}_j'\right) \times$$

$$\times \delta_1 \left(\frac{\left(\bar{v}_i - \bar{v}_j\right)^2 - \left(\bar{v}_i' - \bar{v}_j'\right)^2}{2} \right) d\bar{v}_i' d\bar{v}_j' = \frac{n}{N} \sum_{i<j} \sigma_t(g_{ij}) g_{ij} < \infty \tag{3}$$

and g is the relative collision velocity, $\sigma_t(g_{ij})$ and $\sigma(g_{ij}, \xi_{ij})$ are the total and differential collision cross-sections, and χ_{ij} is the deflection angle.

The total collision frequency (3) determines the time of the next collision in the system and depends on velocities of all particles, and it is necessary to recalculate its value after each collision. This is rather time-consuming if the number of particles N is large, since the summation is performed over all possible $N(N-1)/2$ collision pairs.

Let us introduce the majorant collision frequency [33]

$$\nu_m = \frac{N(N-1)}{2} [g \sigma_t(g)]_{max} \geq \nu(\bar{V}). \tag{4}$$

Then we add to the both sides of eqn (2) the corresponding sides of the equality

$$[\nu_m - \nu(\bar{V})] f_N(t, \bar{V}) = \frac{n}{N} \sum_{i<j} \int f_N(t, \bar{V}') \left\{ [g \sigma_t(g)]_{max} - g_{ij}' \sigma_t(g_{ij}') \right\} \delta(\bar{V} - \bar{V}') d\bar{V}'$$

and join the right-side integrals to have

$$\frac{\partial}{\partial t} f_N(t, \bar{V}) + \nu_m f_N(t, \bar{V}) =$$

$$= \frac{n}{N} \sum_{i<j} \int f_N(t, \bar{V}') \Big\{ \left[[g \sigma_t(g)]_{max} - g_{ij}' \sigma_t(g_{ij}') \right] \delta(\bar{v}_i - \bar{v}_i') \delta(\bar{v}_j - \bar{v}_j') + w(\bar{v}_i', \bar{v}_j' \to \bar{v}_i, \bar{v}_j) \Big\} d\bar{v}_i' d\bar{v}_j'. \tag{5}$$

Here δ denotes Dirac's delta-function.

Let us introduce the function $\psi(t, \bar{V})$ as

$$f_N(t, \bar{V}) \nu(\bar{V}) = \int_0^\infty K_2(t' \to t | \bar{V}) \psi(t', \bar{V}) dt',$$

where K_2 is the kernel

$$K_2(t' \to t | \bar{V}) = \theta(t - t') \nu(\bar{V}) \exp\left\{ -\nu(\bar{V})(t - t') \right\}$$

and θ is the Heaviside function, then eqn (5) may be transformed to an integral form

$$\psi(t,\bar{V}) = \int_0^\infty \int K_{21}\psi(t',\bar{V}')d\bar{V}'dt' + \delta(t)f_N^0(\bar{V}) \tag{6}$$

with the kernel

$$K_{21} = K_2(t' \to t|\bar{V}')K_1(\bar{V}' \to \bar{V}).$$

Here

$$K_2(t' \to t|\bar{V}') = \theta(t-t')\nu_m \exp\{-\nu_m(t-t')\},$$

$$K_1(\bar{V}' \to \bar{V}) = \sum_{i<j} \frac{2}{N(N-1)} \times$$

$$\times \left\{ \left[1 - \frac{g'_{ij}\sigma_t(g'_{ij})}{[g\sigma_t(g)]_{max}}\right] \delta(\bar{v}_i - \bar{v}'_i)\delta(\bar{v}_j - \bar{v}'_j) + \frac{g'_{ij}\sigma_t(g'_{ij})}{[g\sigma_t(g)]_{max}} \frac{w(\bar{v}'_i, \bar{v}'_j \to \bar{v}_i, \bar{v}_j)}{g'_{ij}\sigma_t(g'_{ij})} \right\} \prod_{\substack{m=1 \\ m\neq i,j}}^{N} \delta(\bar{v}_m - \bar{v}'_m).$$

The probability treatment of eqn (6) enables one to construct a random process that describes the behavior of the N-particle gas model. To calculate the initial trajectory point of this process, the free term from eqn (6) is used as the probability density, while the kernel K_{21} yields the probability density of the transition from

$$\text{the state } (t', \bar{V}') \text{ to the state } (t, \bar{V}).$$

This transition is modeled sequentially from

$$\text{the state } (t', \bar{V}') \text{ to } (t, \bar{V}')$$

in accordance with the distribution density $K_2(t' \to t|\bar{V}')$.
Then, in compliance with the kernel $K_1(\bar{V}' \to \bar{V})$ the transition $(t, \bar{V}') \to (t, \bar{V})$ occurs.

For this purpose, a collisional pair (i, j) is uniformly chosen from $N(N-1)/2$ pairs (this is evidenced by the presence of the factor $2/N(N-1)$ in the kernel K_1). A collision of this pair occurs with the probability

$$P = \frac{g'_{ij}\sigma_t(g'_{ij})}{[g\sigma_t(g)]_{max}},$$

and with the probability $(1-P)$ the velocities will not change (this is evidenced by the presence of the product of two delta-functions in the first term of the kernel K_1), i.e. a fictitious collision occurs. The product of delta-functions in K_1 (the last factor) shows that after a collision of the pair (i, j) velocities of other particles remain unchanged, whereas velocities $(\bar{v}'_i, \bar{v}'_j)$ for real collisions are replaced by post-collisional velocities $(\bar{v}_i, \bar{v}_j)$.

Collision impact parameters are selected with the probability

$$\frac{w(\bar{v}'_i, \bar{v}'_j \to \bar{v}_i, \bar{v}_j)}{g'_{ij}\sigma_t(g'_{ij})},$$

and the presence of two delta-functions δ_3 and δ_1 in w (see (3)) shows that new velocities are calculated in accordance with momentum and energy conservation laws.

Thus, all required procedures for trajectory simulation of the random process are specified, and the numerical scheme of the DSMC method is constructed for a spatially uniform case. Its computer cost is proportional to the number of simulated particles [2].

Usually in problems of rarefied gas dynamics it is required to determine gas parameters at the time moment t_k, which have the form

$$I_h(t_k) = \int h(\bar{v}) f_1(t_k \bar{v}) d\bar{v} = \int H(\bar{V}) f_N d\bar{V},$$

where $h(\bar{v})$ is the function of velocity, and

$$H = \frac{1}{N} \sum h(\bar{v}).$$

To calculate functionals, such as $I_h(t_k)$, it is possible to use the estimates known from the general theory of Monte-Carlo methods [40]. In particular, a counterpart of the non-biased absorption estimate has the form

$$\xi_\psi = H(\bar{V}_s), s = max\{n : t_n < t_i, n = 0, 1, ...\}.$$

Approximate values $\tilde{I}_h(t_k)$ of the functionals $I_h(t_k)$ are given by

$$\tilde{I}_h(t_k) = L^{-1} \sum_{l=1}^{L} \xi_\psi(l),$$

where L is the number of independent N-particle trajectories of a random process. Following [33], it can be shown that the mathematical expectation is

$$E[\xi_\psi] = I_h(t_k),$$

and the variance of random variable ξ_ψ is

$$Var\left[\xi_\Psi\right] = N^{-1} \left\{ \int h^2\left(\bar{v}\right) f_1\left(t, \bar{v}\right) d\bar{v} - I_h^2\left(t_k\right) \right\} +$$

$$+ \frac{N-1}{N} \int h\left(\bar{v}_1\right) h\left(\bar{v}_2\right) \left\{ f_2\left(t, \bar{v}_1, \bar{v}_2\right) - f_1\left(t, \bar{v}_1\right) f\left(t, \bar{v}_2\right) \right\} d\bar{v}_1 d\bar{v}_2. \quad (7)$$

It is known [39] that the variance of absorption estimate is limited and, by the central limit theorem, the following inequality is valid:

$$\left| L^{-1} \sum_{l=1}^{L} \xi_\Psi^l - I_h\left(t_k\right) \right| \leq 3 \sqrt{\frac{Var\left[\xi_\Psi\right]}{L}}$$

It is commonly believed that the statistical error of the DSMC method is determined only by the overall volume of the sampling, $(N \cdot L)$. It follows from (7) that under the condition of molecular chaos ($f_2 = f_1 f_1$) the second term vanishes, and the statistical error is proportional to

$$1/\sqrt{N \cdot L}.$$

For finite N, however, there is always a statistical dependence of particles (see [33] for more detail); and, hence, the statistical error is proportional to

$$1/\sqrt{L}.$$

To analyze the relationship between simulation results and the solution of the Boltzmann equation, it is necessary to consider the kinetic equation for the one-particle distribution function

$$f_1(t,\bar{v}_1) = \int f_N(t,\bar{V}_N)d\bar{v}_2...d\bar{v}_N.$$

If Kac MKE equation (1) is integrated over $(N-1)$ variables $v_2,...,v_N$, then we obtain a kinetic equation for the one-particle distribution function

$$\frac{\partial}{\partial t}f_1 = \frac{N-1}{N}\,n\int_0^{2\pi}d\epsilon\int_0^{\infty}b\,db\times$$

$$\times\int d\bar{v}_2|\bar{v}_1-\bar{v}_2|(f_1(\bar{v}_1')f_1(\bar{v}_2')-f_1(\bar{v}_1)f_1(\bar{v}_2))+$$

$$+\frac{N-1}{N}\,n\int_0^{2\pi}d\epsilon\int_0^{\infty}b\,db\int d\bar{v}_2|\bar{v}_1-\bar{v}_2|(g_2'-g_2), \qquad (8)$$

where $g_2 = f_2 - f_1 f_1$. In the general case the solution of equation (8) differs considerably from the solution of the Boltzmann equation, since it depends on the variation of the two-particle correlation function $g_2(t,\bar{v}_1,\bar{v}_2)$. Examples of the influence of statistical dependence of particles on the simulation results were presented in [33]. Equation (8) is transformed into the Boltzmann equation [41] when $N\to\infty$ and the molecular chaos hypothesis is valid. Strictly speaking, only under these conditions the results of statistical simulation precisely correspond to the solution of the Boltzmann equation.

It is shown therefore, that the use of the MKE allows one to obtain not only a probabilistic procedure for simulation of the random process and statistical estimates for calculating the gas parameters, but also to assess the statistical error of results. In addition, the relationship between the results of simulation of the N-particle gas model and the solution of the Boltzmann equation has become more transparent.

The next step is to illustrate how the approach described can be extended to a spatially nonuniform case. The traditional approach [1] employs the discretization of spatial-temporal evolution of the N-particle gas model. A continuous process of motion and collisions of molecules is uncoupled, the computational domain is divided into cells, and the following processes are sequentially simulated at each step Δt:

- spatially uniform relaxation of the gas in each cell;
- free-molecular movement of simulated particles over the distances appropriate to Δt with regard for boundary conditions.

A different approach was proposed by Ivanov and Rogasinsky [2] who constructed numerical schemes for simulating a $6N$-particle, continuous in time, random process of

spatially nonuniform evolution of a system of N particles. These schemes were derived directly from the Leontovich master kinetic equation [4]:

$$\frac{\partial f_N}{\partial t} + \sum_{i=1}^{N} \bar{v}_i \frac{\partial f_N}{\partial \bar{r}_i} f_N = \sum_{i<j} \delta(\bar{r}_i - \bar{r}_j) \int \{f'_N - f_N\} |\bar{v}_i - \bar{v}_j| b_{ij} db_{ij} d\epsilon_{ij}. \tag{9}$$

Here $f_N = f_n(t, \bar{R}, \bar{V})$, $f'_N = f_n(t, \bar{R}, \bar{V}'_{ij})$ are the N-particle distribution functions, and

$$\int f_N d\bar{V} d\bar{R} = 1.$$

The relationship between this equation and spatially nonuniform Boltzmann equation was studied in [5].

The presence of the delta-function in collision integral (9) indicates the collision "locality", i.e. identical coordinates of colliding particles, like in the Boltzmann equation. For numerical simulation one has to perform the regularization of collision integral (9), i.e. introduce "smeared" particle interactions. Using the function w_ρ, the collision integral in eqn (9) takes the form

$$J_N = \sum_{i=j}^{N} \int \left(f'_N - f_N\right) w_\rho d\bar{v}'_i d\bar{v}'_j,$$

where

$$w_\rho \left(\bar{v}'_i, \bar{v}'_j \to \bar{v}_i, \bar{v}_j | \bar{r}_i, \bar{r}_j, \rho\right)$$

is the probability density of transition of the pair (i, j) from the state $(\bar{v}'_i, \bar{v}'_j)$ to the state $(\bar{v}_i, \bar{v}_j)$ with fixed values of particle coordinates $(\bar{r}_i, \bar{r}_j)$ and regularization parameter ρ. In this case,

$$w_\rho \left(\bar{v}'_i, \bar{v}'_j \to \bar{v}_i, \bar{v}_j | \bar{r}_i, \bar{r}_j, \rho\right) \to \delta\left(\bar{r}_i - \bar{r}_j\right) w \left(\bar{v}'_i, \bar{v}'_j \to \bar{v}_i, \bar{v}_j\right) when\, \rho \to 0$$

Let us consider the following regularization

$$w_\rho \left(\bar{v}'_i, \bar{v}'_j \to \bar{v}_i, \bar{v}_j | \bar{r}_i, \bar{r}_j, \rho\right) = h(\bar{r}_i, \bar{r}_j) w \left(\bar{v}'_i, \bar{v}'_j \to \bar{v}_i, \bar{v}_j\right),$$

$$h(r_i, r_j) = \begin{cases} \omega_0^{-1}, & if\ |\bar{r}_i - \bar{r}_j| < \rho, \\ 0, & if\ |\bar{r}_i - \bar{r}_j| > \rho, \end{cases}$$

$$\omega_0 = \frac{4}{3} \pi \rho^3.$$

The parameter ρ defines the dimension of the "interaction region" of particles, and its value depends on the required accuracy of calculation of flow parameters.

Then, the total collision frequency of an N-particle gas model is as follows

$$\nu_\rho(\bar{R}, \bar{V}) = \sum_{i<j}^{N} h(\bar{r}_i, \bar{r}_j) g_{ij} \sigma_t(g_{ij}) < \infty, \tag{10}$$

and it depends on the particle coordinates and velocities. As in the case of a uniform gas model, the calculation of this collision frequency requires the summation of $N(N-1)/2$ pairs with checking the distance between the particles, which is time-consuming. Therefore, here it is again profitable to majorize the collision frequency, and contrary to (4) not only with respect to the particle velocities, but also to the coordinates of colliding particles.

Let us choose the majorant collision frequency in the form

$$\nu_m = \frac{N(N-1)}{2}\omega_0^{-1}[g\sigma_t(g)]_{max} \geq \nu(\bar{R},\bar{V}), \tag{11}$$

and transform the Leontovich equation, similar to the uniform case, to the following form:

$$\frac{\partial f_N}{\partial t} + \sum_{i=1}^{N} \bar{v}_i \frac{\partial f_N}{\partial \bar{r}_i} f_N + \nu_m f_N =$$

$$= \sum_{i<j}^{N} \int f'_N \big\{ h(\bar{r}_i,\bar{r}_j)\omega_0^{-1} w(\bar{v}'_i,\bar{v}'_j \to \bar{v}_i,\bar{v}_j) +$$

$$+ \big([g\sigma_t(g)]_{max}\omega_0^{-1} - h(\bar{r}_i,\bar{r}_j)\omega_0^{-1} g_{ij}\sigma_t(g_{ij})\big) \times \delta(\bar{v}'_i - \bar{v}'_i)\delta(\bar{v}'_j - \bar{v}'_j)\big\} d\bar{v}'_i d\bar{v}_j. \tag{12}$$

The collision integral here consists of two parts corresponding to real (first term) and fictitious (second term) collisions.

The use of such a majorant collision frequency ν_m allows one, therefore, to transform the nonuniform problem under consideration to a spatially uniform problem with a constant collision frequency.

If eqn (12) with appropriate initial and boundary conditions is transformed to a linear integral equations (see details in [2]), then the probability treatment of the kernel and free term of this equation allows for formulating a new scheme of direct statistical simulation of spatially nonuniform rarefied gas flow with continuous time.

Below, the salient points in simulation of a $6N$-dimensional trajectory of the random process of the transition of an N-particle system from the state $(t', \bar{R}', \bar{V}')$ to $(t, \bar{R}, \bar{V})$ are briefly described.

We shall not dwell here upon the simulation of particles entering the computational domain and the interaction of particles with the body surface. All details can be found in [2].

The time of the next collision t has the probability density distribution

$$\nu_m \exp\left\{-\nu_m(t-t')\right\},$$

while the probability density of the transition of a system of N particles from the state $(t', \bar{R}', \bar{V}')$ to $(t, \bar{R}, \bar{V}')$ is the delta-function

$$\delta(\bar{R} - \bar{R}' - \bar{V}'(t-t')).$$

This means that all simulated particles move during the time $t - t'$ from point $\bar{R}'$ to $\bar{R}$ with velocities $\bar{V}'$.

An examination whether the collision is real is performed as follows:
if $|\bar{r}_i - \bar{r}_j| > \rho$ **then** the collision is fictitious, **else** the collision is real with the probability

$$\frac{g_{ij}\sigma_t(g_{ij})}{[g\sigma_t(g)]_{max}}$$

and fictitious with the complementary probability.

Thus, all probabilistic procedures necessary for the numerical generation of the trajectories of a $6N$-dimensional random process of evolution of a spatially nonuniform N-particle gas model are described.

For regularization of the collision integral in eqn (9) it is also possible to use a usual approach of the DSMC method: the computational domain is divided into non-intersecting cells d_k, so that

$$\sum_{k=1}^{M} d_k = V_0,$$

and a collision may occur only between particles that belong to the same cell. Then the majorant collision frequency has the form

$$\nu_m = \frac{N(N-1)}{2}[g\sigma_t(g)]_{max} d_{min}^{-1}, d_{min} = min(d_k). \tag{13}$$

A collision of the pair (i, j) randomly chosen from all $N(N-1)/2$ pairs is fictitious if the particles i and j are in different cells.

The use of the majorant collision principle for spatially nonuniform case with the regularization of the type (11) or (13) allows one, therefore, to obtain a new exact time-continuous scheme of the DSMC method.

A salient point that differs this scheme from the conventional DSMC method is the transfer of all particles after each collision. Certainly, this is extremely expensive; therefore, only examples of using this algorithm for 1D rarefied gas dynamic problems (shock wave structure and Couette flow) are now available. However, the mere fact that it is possible to simulate rarefied gas flows, avoiding uncoupling of a continuous process of molecular motion and collisions, is of principal importance. Possibly, this approach can be used in future when the computer performance significantly increases.

It is natural to consider an approximate simulation scheme with separated and sequentially calculated collisions and motions of particles.

Let us introduce discrete time instants $t_n = n \cdot \Delta t$ and choose a step Δt such that for each τ_m, provided $\sum_m \tau_m \leq \Delta t$, the following condition is valid:

$$\nu_\rho\left(\bar{R} + \tau_m \cdot \bar{V}, \bar{V}|\rho\right) \approx \nu_\rho\left(\bar{R}, \bar{V}|\rho\right)$$

This means that the change in collision probability of pairs due to particle displacement is ignored during the time Δt. Then an approximate simulation scheme is as follows: the time between consecutive collisions is chosen on the basis of the probability density

$$\nu_m \exp\left\{-\nu_m(\tau)\right\}.$$

If

$$\sum \tau_m^l < \Delta t,$$

then a collision (real or fictitious) occurs. All particles are displaced at a distance proportional to Δt one time, at the end of the step Δt.

Numerical schemes with a continuous and discrete time that make use of the majorant collision frequency with the regularization of types (11) or (13) do not employ the sorting of particles over cells and, therefore, can be called free cell schemes. The determination of distributed and total aerodynamic characteristics can be conducted directly using only the collisions of a particle with the body surface. The calculation of flowfields requires a grid for sampling the gas parameters, but this grid is not related to collision simulation.

The value of the free cell majorant can be reduced by sorting the particles over the cells. Then

$$\nu_m = \sum_{k=1}^{M} \nu_m^k = \sum_{k=1}^{M} \frac{N_k(N_k-1)}{2} \frac{[g\sigma_t(g)]_{max}^k}{d_k}, \tag{14}$$

where N_k is the number of molecules in the k-th cell. Obviously,

$$\nu_m^{cell} < \nu_m^{freecell}$$

and, hence, the computational cost of the cell scheme is smaller than that of the free cell scheme. In the cell scheme, however, it is necessary to take into account the cost of particle sorting over cells. This sorting is very simple in the case of a rectangular Cartesian grid, but with using more complex adaptive body-fitted grids its cost drastically increases.

When using the cell regularization with the majorant (14), having determined the time of the next collision τ_m^l at the step Δt, one has to determine the number of the cell in which this collision occurs. The cell number, k, is selected with the probability ν_m^k/ν_m. Then a pair (i,j) is uniformly chosen in the k-th cell from N_k particles. The collision is real with the probability

$$\frac{g_{ij}\sigma_t(g_{ij})}{[g\sigma_t(g)]_{max}}$$

and fictitious with the complementary probability.

The mean number of collisions in a system of N particles during the time Δt is $\nu_m \Delta t$, and each cell is chosen with the probability ν_m^k/ν_m. Consequently, during the time Δt each cell is chosen $\nu_m^k \Delta t$ times in the average. Then for $\nu_m^k \Delta t \gg 1$ there is no need to sample the cell number, and the usual sequential computation of collisions over all cells can be employed.

The scheme that uses the cell regularization with particle sorting and probabilistic choice of the cell number where a collision will occur can be called a cell majorant collision frequency scheme.

Our experience of using the cell and free cell schemes, which has been accumulated up to now, shows that these schemes should not be set in opposition. Vice versa, it is desirable to use them together. For this purpose, the computational domain is divided into uniform Cartesian cells with the linear dimension of the order of λ_∞, and the cell scheme is used there. In flow areas where the local mean free path strongly decreases and in the vicinity of the body surface, the free cell scheme is used with a small regularization parameter in order to increase the spatial collision resolution.

Now a few words about the influence of the finite number of simulated particles on the results of computations. In the nonuniform case, the main criterion that allows for a practical verification of the presence of a statistical dependence between the simulated

particles is the relative number of repeated collisions. Here, repeated collisions are collisions between the same pair of particles during their lifetime in the computational domain. This number is directly related to the number of particles N_λ in a volume with linear size of the local mean free path. If $N_\lambda \geq 1$, we can definitely say that the simulation results are close to the solution of the Boltzmann equation.

This is certainly only an intuitive, experience-based criterion. A more detailed study of the influence of statistical dependence with the use of autocorrelation functions and the number of repeated collisions can be found in [42].

The extension of the majorant collision frequency schemes, directly obtained from the MKE, to the case of multi-species chemically reacting mixtures is straightforward. It implies the change in cross-sections of the corresponding inelastic processes and, hence, the change in the collisional algorithm only in its part that refers to collision mechanics.

A Appendix 2. Gas/surface interaction models

Calculation of aerodynamic forces by the DSMC method requires setting the velocity distribution functions for molecules reflected from the object surface. A simplified representation of this function is used, which must take into account the major features of gas-surface interaction which have been revealed in experiments (force action, angular distribution of molecules escaped), on the one side, and it must be simple enough in application, on the other side.

The main requirement of the surface properties definition is to introduce for every element of the space object the following surface properties:

1. Wall temperature

2. Scheme of gas-surface interaction (Maxwell or Nocilla) model, accommodation and interaction coefficients.

If a space object consists of several hundred or thousand elements it is not convenient for user to introduce or edit the properties of each element. So a procedure was found to give the user a fast possibility for introducing and editing with a maximum flexibility:

1. Setting surface properties for the geometric model. For each compound and element a list of surface properties can be assigned.

2. Introducing and checking the surface properties of a compound. The system shows the actual content of this compound and to each element surface properties can be assigned.

3. To check the correct settings of the surface properties the system provides a visualization tool.

One of the oldest and most widely used distribution functions for the reflected molecules is due to *Maxwell* [43].

It is constructed on the assumption that a fraction $1 - \sigma$ of the molecules is reflected from the surface in a specular fashion, while the fraction σ is re-emitted diffusely, with the Maxwellian distribution:

$$f_r(\vec{r}, \vec{\xi_r}) = (1 - \sigma)\ f_i\ (\vec{r}, \vec{\xi_r} - 2(\vec{\xi_r} \cdot \vec{n})\vec{n}) + \sigma\ \pi^{-3/2}\ c_r'^{-3}\ exp\left\{-\frac{\vec{\xi_r^2}}{c_r'^2}\right\}$$

where $\vec{\xi_r}$ is the reflected velocity $\vec{n}$ is the external normal of the surface in point $\vec{r}$, c_r' is the most probable speed at the temperature T_r.

The parameter σ is called the tangential momentum accommodation coefficient. Evidently, for completely specular reflection, $\sigma = 0$, while for complete diffuse reflection, $\sigma = 1$.

This implementation of the specular-diffuse scheme implies either specular or diffuse reflection of particles. Therefore, at first, each particle is sampled to experience a particular type of reflection. If the pseudo-random number is smaller than σ, the particle experiences diffuse reflection; otherwise, it experiences specular reflection.

In the case of specular reflection, the velocity component normal to the surface changes its sign, and the tangential components of velocity remain unchanged.

The velocity of diffusely reflected molecules is sampled in the local polar coordinate system, directed along the outer normal of the to surface of the vehicle, in the following manner:

$$| \vec{\xi_r} | = c'_r \sqrt{-\ln(R_1 R_2)};$$
$$\cos(\psi) = \sqrt{R_3};$$
$$\phi = 2\,\pi\,R_4,$$

where $| \vec{\xi_r} |$ - module of the velocity of reflected particle; ψ, ϕ - polar and azimuthal angles and R_1, R_2, R_3, R_4 are random numbers;

Following ref.[43] an energy accommodation coefficient $\sigma_E = \frac{E_i - E_r}{E_i - E_w}$ is used. When the accommodation coefficient $\sigma_E = 0$ then the molecules don't exchange energy with the wall, and $\sigma_E = 1$ if the incident molecules reached thermal equilibrium with the wall.

If we write the energy of a molecule in terms of its velocity, Eq. A takes the form:

$$\sigma_E = \frac{\xi_i^2 - V_r^2}{\xi_i^2 - {c'}_r^2};$$

accordingly, the value of velocity with which the particles are reflected is written as

$$V_r = \sqrt{(1 - \sigma_E)\xi_i^2 + \sigma_E {c'}_r^2}$$

Thus, for each diffusely reflected molecule, the absolute value of its sampled velocity $| \vec{\xi_r} |$ should be corrected by the coefficient

$$k = \frac{V_r}{{c'}_r} = \sqrt{(1 - \sigma_E)\xi_i^2 / {c'}_r^2 + \sigma_E},$$

and hence

$$| \vec{\xi_r} | = k c'_r \sqrt{-\ln(R_1 R_2)}.$$

The distribution function [44-45] for the velocities of reflected particles which is often used in practice has the following form:

$$f_r = n_r \left(\frac{1}{\pi}\frac{m}{2kT_r}\right)^{\frac{3}{2}} exp\left\{-\frac{m}{2kT_r}\left[\vec{\xi} - \vec{U_r}\right]^2\right\} =$$

$$= n_r \left(\frac{1}{\pi}\frac{m}{2kT_r}\right)^{\frac{3}{2}} exp\left\{-\left[\left(\frac{m}{2kT_r}\right)^{\frac{1}{2}}\vec{\xi} - \vec{S_r}\right]^2\right\} =$$

$$= n_r \left(\frac{1}{\pi}\frac{m}{2kT_r}\right)^{\frac{3}{2}} exp\left\{-\left[\left(\frac{m}{2kT_r}\right)^{\frac{1}{2}}\xi_y - S_{nr}\right]^2 - \left[\left(\frac{m}{2kT_r}\right)^{\frac{1}{2}}\xi_x - S_{\tau r,x}\right]^2 - \left[\left(\frac{m}{2kT_r}\right)^{\frac{1}{2}}\xi_z - S_{\tau r,z}\right]^2\right\}$$

Here m and $\vec{\xi}$ are the mass and velocity of molecules reflected from surface, and parameters of particle number density n_r, temperature T_r and speed $\vec{U_r}$ depend on the

velocity vector of a molecule incident upon the surface, as well as on its energy, surface characteristics and total mass flow of incident molecules. These dependences transform to those of five scalar parameters of function f_r on the base of available experimental data and mass conservation law.

The experiments [44] showed that the vector of the mean reflected velocity is located in the same plane as the vector of the incident velocity. Thus, if we construct the right-hand Cartesian coordinate system at the point of particle reflection so that the x axis is the projection of the incident velocity vector onto a plane tangential to the surface, the y axis coincides with the external normal to the surface, then the side component of reflected velocity is $S_{\tau r,z} = 0$.

The four parameters of this function S_{nr}, $S_{\tau r,x}$, T_r, n_r are found[44,45] as follows:

$$S_{nr} = 0.1 - 0.65\frac{2\theta}{\pi},$$

$$S_{\tau r,x} = \frac{\tau_{r,x}}{p_r} \cdot \frac{J_2(S_{nr})}{J_1(S_{nr})},$$

$$2\frac{k}{m}T_r = \left(\frac{p_r}{q_{mr}}\right)^2 \left[\frac{J_1(S_{nr})}{J_2(S_{nr})}\right]^2,$$

$$n_r = q_{mr}\left(2\frac{k}{m}T_r\right)^{-\frac{1}{2}} J_1^{-1}(S_{nr}),$$

$$\tau_{r,x} = -\left(a_\tau + b_\tau\frac{4\theta - \pi}{2\pi}\right)\xi\, sin(\theta)\; q_{mi}$$

$$p_r = \left\{\left(a_n + b_n\frac{2\theta}{\pi}\right)\xi + \left(\frac{\pi}{2}\frac{kT_w}{m}\right)^{\frac{1}{2}}\right\}\; q_{mi}$$

$$J_1(t) = \frac{1}{\sqrt{\pi}}\int_0^\infty q\, exp\left[-(q-t)^2\right]\, dq = \frac{1}{\sqrt{2\pi}}\left[e^{-t^2} + \sqrt{\pi}\, t\,(1 + erf(t))\right],$$

$$J_2(t) = \frac{1}{\sqrt{\pi}}\int_0^\infty q^2\, exp\left[-(q-t)^2\right]\, dq = \frac{1}{\sqrt{2\pi}}\left[te^{-t^2} + \sqrt{\pi}\,(\frac{1}{2} + t^2)\,(1 + erf(t))\right],$$

$$erf(t) = \frac{2}{\sqrt{\pi}}\int_0^t e^{-s^2}\, ds,$$

$$q_{mr} = q_{mi} = m\, q_1;\;\; q_1 = 1[m^{-2}\, s^{-1}].$$

Here θ is the angle between the incident velocity vector and internal normal to the surface, T_w is the surface temperature, q_{mr} and q_{mi} are the fluxes of reflected and incident molecules, which is used to normalize the distribution function f_r in the Monte-Carlo method.

The values of model parameters a_n, b_n, a_τ, and b_τ depend on the type of material, and the following values were obtained [44,45] based on experimental data:

Materials	a_n	b_n	a_τ	b_τ
Ceramics	0.06	0.05	-0.03	0.26
White enamel	0.07	0.10	-0.01	0.16
Black enamel	0.065	0.08	-0.03	0.11
Scree-vacuum glass Cloth	0.07	0.03	-0.05	0.11
Anodized aluminium-magnesium Alloy (AMA)	0.10	0.10	-0.06	0.04
Chemically polished AMA	0.11	0.18	-0.19	-0.04
Glasses	0.17	0.09	-0.10	-0.08
Enamels	0.07	0.06	-0.01	0.12

Sampling of velocity with which a particular particle is reflected involves the probability density of reflected molecules, which is obtained from the distribution function and is written in the following form:

$$F_{r,x} = \frac{1}{\sqrt{\pi}\sqrt{T_r}} exp\left\{ - \left[\left(\frac{m}{2kT_r} \right)^{\frac{1}{2}} \xi_x - S_{\tau r,x} \right]^2 \right\}$$

$$F_{r,y} = \frac{2}{\sqrt{\pi}\sqrt{T_r}\, J_1(S_{nr})} \left(\frac{m}{2kT_r} \right)^{\frac{1}{2}} \xi_y \, exp\left\{ - \left[\left(\frac{m}{2kT_r} \right)^{\frac{1}{2}} \xi_y - S_{nr} \right]^2 \right\}$$

$$F_{r,z} = \frac{1}{\sqrt{\pi}\sqrt{T_r}} exp\left\{ - \left[\left(\frac{m}{2kT_r} \right)^{\frac{1}{2}} \xi_z \right]^2 \right\}$$

The velocity ξ_y is simulated by the Neumann method, and the velocities ξ_x and ξ_z are simulated on the basis of the relations

$$\frac{\xi_x}{c'_r} = \sqrt{-\ln(R_1)}\, cos(2\pi\, R_2) \; + \; S\tau r, x$$

$$\frac{\xi_z}{c'_r} = \sqrt{-\ln(R_1)}\, sin(2\pi\, R_2)$$

where R_1 and R_2 are pseudo-random numbers.

References

[1] Bird, G. A., *Molecular gas dynamics and the direct simulation of gas flows*, Clarendon press, Oxford, 1994.

[2] Ivanov MS, Rogasinsky SV. 1991. Theoretical analysis of traditional and modern schemes of the DSMC method. *Proc. 17th Int. Symp. on Rarefied Gas Dynamics, Aachen, pp. 629-642*, ed. AE Beylich, VCH

[3] Kac M. 1959. *Probability and related topics in the physical sciences*, Interscience, New York

[4] Leontovich, M. A., Soviet Physics JETP, 5, 211-231 (1935).

[5] Klimontovich, Yu. L., Uspehi Fiz. Nauk, 139, No. 4, 689-700 (In Russian) (1983).

[6] Koura, K., Phys. Fluids, 29, 3509-3511 (1986).

[7] Ivanov, M. S. , Markelov, G. N., Gimelshein, S. F., AIAA Paper 98-2669 (1998).

[8] Markelov, G. N., Ivanov, M. S., Journal of Spacecraft and Rockets, 38, No. 6, 875-881 (2001).

[9] Ivanov, M.S., Markelov, G.N., Gimelshein, S.F. Mishina, L.V. Krylov, A.N, Greckho, N.V., 1998, '*"High Altitude Capsule Aerodynamics with Real Gas Effects"*, J. of Spacecraft and Rockets, Vol.35. No. 1., pp.16-22.

[10] Haas, B. L., Boyd, I. D., AIAA Paper 91-0774 (1991).

[11] Koura, K., Phys. Fluids A, 4, No. 8, 1782-1788 (1992).

[12] Boyd, I. D., Phys. Fluids A, 5, No. 9, 2278-2286 (1993).

[13] Gimelshein, S. F., Gorbachev, Yu. E., Ivanov, M. S., Kashkovsky, A. V., Proc. of 19 Int. Symp. on Rarefied Gas Dynamics, Oxford University Press, 1995, Vol. 1, pp. 556-563.

[14] Boyd, I. D., Phys. Fluids A, 8, No. 5, 1293-1300 (1996).

[15] Koura, K., Matsumoto, H., Phys. Fluids A, 3, No. 10, 2459-2465 (1991).

[16] Gimelshein, S. F., Boyd, I. D., Ivanov, M. S., AIAA Paper 99-3451 (1999).

[17] Borgnakke, C., and Larsen, P. S., J. Comp. Phys., 18, No. 4, 1975, 405-420 (1975).

[18] Lumpkin, F. E., Haas, B. L., Boyd, I D., Phys. Fluids A, 3, No. 9, 2282-2284 (1991).

[19] Haas, B. L, Hash, D., Bird, G. A., Lumpkin, F. E., Hassan, H., Phys. Fluids A, 6, No. 6, 2191-2201 (1994).

[20] Gimelshein, S. F., Gimelshein, N. E., Levin, D. A., Ivanov, M. S., Markelov, G. N., AIAA Paper 2002-2759 (2002).

[21] Bergemann, F., Boyd, I. D., Rarefied Gas Dynamics: Theory and Simulations, 158, 1994, edited by B. D. Shizgal and D. P. Weaver, Progress in Astronautics and Aeronautics, 1994, pp. 174-183

[22] Choquet, I., *Modelisation des desequilibres thermiques dans les ecoulements de gas rarefies*, Ph.D. thesis, L'universite Paris VI, (1993).

[23] Millikan, R. C., White, D. R., J. Chem. Phys., 39, No. 12, 3209-3213 (1996).

[24] Marriott, P. M., Non-equilibrium chemical reactions in the simulation of hypersonic rarefied flows, Ph.D. thesis, Imperial College of Science, Technology and Medicine, London, (1994).

[25] Gimelshein, S. F., Ivanov, M. S., Markelov, G. N., Gorbachev, Yu. E., "Quasiclassical VRT transitional models in the DSMC computations of reacting flows", Proc of the 20 Int. Symp. on Rarefied Gas Dynamics, Beijing (1996).

[26] Koura, K., *"Rotationally and vibrationally inelastic cross-section models for direct simulation Monte Carlo methods"*, Proc. of the 20 Int. Symp. on Rarefied Gas Dynamics, Beijing (1996).

[27] Gimelshein, N. E., Gimelshein, S. F, Levin, D. A. "Vibrational relaxation rates in the direct simulation Monte Carlo method", Physics of Fluids.

[28] Bird, G.A., "Simulation of Multi-Dimensional and Chemically Reacting Flows," Rarefied Gas Dynamics, 1, edited by R. Campargue, COMMISSARIAT A LENERGIE ATOMIQUE-Paris, 1979, pp. 365-388.

[29] Wysong, I. J., Dressler, R. A., Chiu, Y. H., Boyd, I. D., AIAA Paper 2000-2359 (2000).

[30] Markelov, G. N., Kudryavtsev, A. N., Ivanov, M. S., Proc. of 21 Int. Symp. on Rarefied Gas Dynamics, Cepadues Editions, 1, 647 (1999).

[31] Markelov, G. N., Kudryavtsev, A. N., Ivanov, M. S., AIAA Paper 99-3527 (1999).

[32] Markelov, G. N., Kudryavtsev, A. N., Ivanov, M. S., Journal of Spacecraft and Rockets, 37, No. 4, 499-506 (2000).

[33] Ivanov MS, Rogasinsky SV, Rudyak VYa. 1989. Direct statistical simulation method and master kinetic equation. In *Rarefied Gas Dynamics, vol. 118, pp. 171-181*, ed. EP Muntz, D Weaver, D Campbell, Progress in Astronautics and Aeronautics

[34] Gimelshein, S. F., Ivanov, M. S., Rogasinsky, S. V., Proc. of the 17 Int. Symp. on Rarefied Gas Dynamics, Aachen, 718-726 (1991).

[35] Gimelshein S.F., Levin D.A., Markelov G.N., Kudryavtsev A.N., Ivanov M.S. AIAA Paper 2002-0736.

[36] Ivanov, M. S., Bondar, Ye. A., Markelov G. N., Gimelshein, S. F., and Taran, J.-P., "Study of the shock wave structure about a body entering the Martian atmosphere", to be published in Proc. of the 23 Int. Symp. on Rarefied Gas Dynamics, Whistler, Canada, July 2002.

[37] Ivanov MS, Rogasinsky SV. 1988. Analysis of the numerical techniques of the direct simulation Monte Carlo method in the rarefied gas dynamics. *Soviet J. Numer. Anal. Math. Modelling*, 3(6):453-465

[38] Moss, J. N., Olejniczak, J., AIAA Paper 98-2668 (1998).

[39] Mikhailov GA. 1995. *New Monte Carlo methods with estimating derivatives*, VCP, Utrecht, The Netherlands. 186 pp.

[40] Spanier J, Gelbard EM. 1969. *Monte Carlo principles and neutron transport problems*, Addison-Wesley Pub Co., Reading, Mass.

[41] Kac M. 1973. Some probabilistic aspects of the Boltzmann equation. *Acta Physica Austriaca*, 10:379-400

[42] Gimelshein SF, Ivanov MS, Rogasinsky SV. 1991. Investigation of shock wave structure by majorant cell and free cell schemes of DSMC. *Proc. 17th Int. Symp. on Rarefied Gas Dynamics, Aachen, pp. 718-726*, ed. AE Beylich, VCH

[43] Kogan M.N., Rarefied Gas Dynamics Moskow: Nauka, 1967 (transl. 1969, ed.Trilling. New York, Plenum Press)

[44] Musanov S.V., Nikiforov A.P., Omelik A.I., O.G. Freedlander, Experimental Determination of Momentum Transfer Coefficients in Hypersonic Free Molecule Flow and Distribution Function Recovery of Reflected Molecules, Rarefied Gas Dynamics, Ed. O.M. Belotserkovsky et al, 1985, V. 1, pp. 669-676

[45] Freedlander O.C., Nikiforov A.P. "Modelling Aerodynamic Atmospheric Effects on the Space Vehicle Surface Based on Test Data", Proceedings of the 2nd Int. Symp. Environmental Testing for Space Programmes held at ESTEC, 12-15 October 1993, pp. 307-312

[46] V.M. Kotov, E.N. Lychkin, A.G. Reshetin, and A.N. Shelkonogov. An approximate method of aerodynamics calculation of complex shape bodies in a transition region. In Proc. 13th Int. Conf. on Rarefied Gas Dynamics, volume 1, pages 487-494. Plenum Press, 1982.

[47] P. Vashchenkov, M. Ivanov and A. Krylov, Numerical Simulations of High-Altitude Aerothermodynamics of a Promising Spacecraft Model. Proc of 27-th International symposium on Rarefied Gas Dynamics, 2010.